TU Delft

Delft University of Technology

The Nature and Catalytic Function of Cation Sites in Zeolites a Computational Perspective

Li, Guanna; Pidko, Evgeny A.

DOI
10.1002/cctc.201801493

Publication date
2018

Document Version
Final published version

Published in
ChemCatChem

Citation (APA)
Li, G., & Pidko, E. A. (2018). The Nature and Catalytic Function of Cation Sites in Zeolites: a Computational Perspective. *ChemCatChem*. https://doi.org/10.1002/cctc.201801493

Important note
To cite this publication, please use the final published version (if applicable).
Please check the document version above.

Copyright
Other than for strictly personal use, it is not permitted to download, forward or distribute the text or part of it, without the consent of the author(s) and/or copyright holder(s), unless the work is under an open content license such as Creative Commons.

Takedown policy
Please contact us and provide details if you believe this document breaches copyrights.
We will remove access to the work immediately and investigate your claim.

This work is downloaded from Delft University of Technology.
For technical reasons the number of authors shown on this cover page is limited to a maximum of 10.

ChemPubSoc Europe

DOI: 10.1002/cctc.201801493

CHEMCATCHEM Reviews

The Nature and Catalytic Function of Cation Sites in Zeolites: a Computational Perspective

Guanna Li[a] and Evgeny A. Pidko*[a, b]

Zeolites have a broad spectrum of applications as robust microporous catalysts for various chemical transformations. The reactivity of zeolite catalysts can be tailored by introducing heteroatoms either into the framework or at the extraframework positions that gives rise to the formation of versatile Brønsted acid, Lewis acid and redox-active catalytic sites. Understanding the nature and catalytic role of such sites is crucial for guiding the design of new and improved zeolite-based catalysts. This work presents an overview of recent computational studies devoted to unravelling the molecular level details of catalytic transformations inside the zeolite pores. The role of modern computational chemistry in addressing the structural problem in zeolite catalysis, understanding reaction mechanisms and establishing structure-activity relations is discussed. Special attention is devoted to such mechanistic phenomena as active site cooperativity, multifunctional catalysis as well as confinement-induced and multisite reactivity commonly encountered in zeolite catalysis.

Introduction

Zeolites are microporous aluminosilicates with uniform microporous structures, high crystallinity, structural diversity, and large surface area. Zeolites have been extensively studied targeted at applications in such technological areas as catalysis, separation, and adsorption. Historically, zeolite-based catalysts are the work-horses of petrochemical industry and automotive exhaust abatement. The broad range of their technological applications stems from the excellent thermal and chemical stabilities of these materials, their large surface areas, the availability of diverse topologies and versatile chemical properties.[1] For example, zeolite Y with faujasite topology is the active component in the catalyst enabling such crucial petrochemical processes as the fluidized catalytic cracking (FCC) and alkylation.[2] MFI-type zeolites (ZSM-5) find application in such hydrocarbon upgrading processes as the isomerization, oligomerization, cracking, and others.[3] In the past decades, zeolites and zeolite-based materials have been extensively investigated as the catalysts for the valorization of alternatives to oil feedstocks including natural gas[4] and biomass.[5]

The three-dimensional crystalline frameworks of zeolites are represented by networks of molecular-sized channels and cages comprised of corner-shared tetrahedral [TO_4] (T = Si or Al) primary building blocks.[6] By varying the connectivity of such building blocks families of microporous materials with different topologies can be obtained. A negative charge can be introduced onto the framework via the isomorphous substitution of a framework tetravalent silicon by a trivalent aluminum atom. The overall charge neutrality is then achieved by the introduction of cationic species compensating for the resulting negative lattice charge. When such a charge-compensation is provided by protons, Brønsted acid sites (BASs) are formed rendering the resulting H-forms of zeolites strong solid Brønsted acids. These materials find application in such acid-catalyzed reactions as isomerization, alkylation, dehydrogenation, dehydration, and cracking.[7] Despite the well-resolved structure of the zeolitic BAS, it remains a great challenge to establish a quantitative structure-reactivity relationship for this class of materials.[8] The catalytic reactivity of BAS confined in zeolites is determined not only by their intrinsic chemistry but also by the specific topologic features of the zeolite matrix incorporating them. This represents the key difference with the conventional homogeneous Brønsted acid catalysts, for which straightforward acidity-reactivity relationship can be easily established.[9] Furthermore, the substantial heterogeneity of practical zeolite materials, i.e. the presence of lattice defects and other structural inhomogeneities, additionally complicates the formulation of structure-activity relation in zeolite catalysis based solely on the experimental data.[9c,10]

The acidic protons inside zeolite micropores can be replaced by other cationic species including transition metal-containing complexes or multinuclear species giving rise to well-defined Lewis acid or/and redox sites in zeolite micropores. Engineering of defined transition metal catalysts confined in zeolite pores has been recently reviewed in ref. [11]. Such species can bring about new catalytic functionalities expanding thus the scope of application of the zeolite catalysts. For example, the modifica-

[a] Dr. G. Li, Prof. E. A. Pidko
Department Chemical Engineering
Delft University of Technology
Van der Maasweg 9
Delft 2629 HZ (The Netherlands)
E-mail: e.a.pidko@tudelft.nl
[b] Prof. E. A. Pidko
ITMO University
Lomonosova str. 9
St. Petersburg 191002 (Russia)

This manuscript is part of the Anniversary Issue in celebration of 10 years of ChemCatChem.

© 2018 The Authors. Published by Wiley-VCH Verlag GmbH & Co. KGaA. This is an open access article under the terms of the Creative Commons Attribution Non-Commercial License, which permits use, distribution and reproduction in any medium, provided the original work is properly cited and is not used for commercial purposes.

tion of zeolites with transition metal ions, e.g. with Cu^{2+}, $Fe^{2+/3+}$, Co^{2+} or Mn^{2+} bring about the redox activity needed for such important processes as the selective methane oxidation,[4a,12] catalytic NO_x reduction[13] and the catalytic conversion of biomass-derived oxygenates.[14] The introduction of Ga^{3+} or Zn^{2+} gives rise to strong Lewis acid sites that are active in dehydrogenation and dehydroaromatization of light alkanes.[15]

An alternative route to well-defined Lewis acid sites (LASs) in zeolites is via the selective lattice modification through isomorphous substitution of silicon atoms in the framework with other tetravalent elements such as Sn^{4+}, Ti^{4+} or Zr^{4+}.[16] The incorporation of titanium ions into the MFI zeolite yields the so-called TS-1 that is a highly active catalyst in epoxidation olefins with hydrogen peroxide as an oxidant.[17] The presence of well-defined Sn^{4+} sites embedded in the microporous silicious frameworks of zeolites render zeo-type stannosilicates important catalytic materials for biomass upgrading and green organic synthesis applications.[18]

The intrinsic reactivity of the guest catalytic ensembles is not the sole factor determining their chemical reactivity and catalytic behavior. Secondary effects such as the distribution of the active site in the zeolite pores and their local density, the geometrical properties of the confinement space and the chemical properties of the stabilizing zeolite lattice all can substantially affect the properties of the confined catalytic sites. The structural complexity of the practical zeolite catalysts makes the unambiguous determination of the active site structure very challenging. Modern computational chemistry provides powerful tools to elucidating the structures of catalytic species and unravelling the fine details of reaction mechanisms inside the zeolite pores.[19] The development of multi-step protocols combining the highly accurate post-Hartree Fork methods with density functional theory (DFT) calculations offers the possibility of reaching near-chemical accuracy in calculation of thermodynamic and kinetic parameters for elementary steps inside the zeolite pores.[20] The modern "operando" modeling approaches allow accounting for the effects of the reactive environment on the structure and reactivity of zeolite catalysts.[21] For example, the stabilities of different cationic ensembles inside the zeolite pores under varied reaction conditions can readily be assessed via the *ab initio* thermodynamic analysis (aiTA) approach.[22] The dynamic and evolution of intrazeolite species under reaction conditions can directly be followed by ab initio molecular dynamics (aiMD). In conjunction with rare-event sampling techniques, such as metadynamics,[23] umbrella sampling,[24] blue moon sampling[25] and quasiclassical trajectory simulations (QCT),[26] such approaches provide powerful tools to directly map reaction free energy surfaces under the catalytically relevant conditions.

In this Review, we present an overview of recent computational studies addressing the fundamental aspects of catalysis by zeolites. Special focus is laid on addressing structural and mechanistic complexity of zeolite catalysis associated with the presence of guest metal species in confined space of zeolite micropores. The Review is organized as follows. It begins with the discussion on the recent computational studies on Brønsted acidic zeolites. Here, the generic structural problem of zeolite catalysis is illustrated by recent works providing a computational insight into the sitting and distribution of aluminum in zeolite frameworks. The mechanistic complexity of zeolite catalysis is then introduced in a discussion of the role of the secondary interactions and dynamic effects on zeolite acidity. The mechanism of acidity enhancement due to the presence of extraframework cations in zeolite pores is also discussed in this section. Next section presents the recent progress in computational studies aimed at unravelling structure, location, stability and reactivity of Lewis acidic cationic species in zeolite catalysis. This is followed by a section devoted to the discussion of the cooperative reaction mechanisms commonly encountered in zeolite catalysis. An overview of the recent studies highlighting the catalytic role of the Lewis acid-base synergy and direct cooperation between Lewis acid and Brønsted acid sites is presented. In the final section we discuss the role of confinement effects including such phenomena as molecular recognition and multiple-site reactivity in zeolite catalysis. The Review is concluded with a brief summary outlining the challenges and opportunities for computational modelling in zeolite catalysis.

Brønsted Acidity of Zeolites

The distribution, concentration and strength of the BASs are the three most important parameters determining the catalytic activity of acidic zeolites. The size and geometry of the pores

Guanna Li received PhD degrees from Dalian Institute of Chemical Physics and Eindhoven University of Technology supported by the Programme for Strategic Scientific Alliances between China and Netherlands. Afterwards she continued as a postdoc at Eindhoven University of Technology, where she worked on theory of catalytic conversions of natural gas and biomass. In 2016 she received a prestigious VENI award from Netherlands Organization for Scientific Research (NWO) and joined Delft University of Technology as a postdoc to pursue independent research in computational catalysis on the topics related to catalytic chemistry of C1 conversions.

Evgeny A. Pidko received his PhD from Eindhoven University of Technology in 2008, wherein in 2011–2017 he was an Assistant Professor of Catalysis for Sustainability. Since 2016 he has been a part-time Professor of Theoretical Chemistry at ITMO University, St. Petersburg. Since Fall 2017 he has been an Associate Professor and head of the Inorganic Systems Engineering group at Delft University of Technology. In his research he combines theory and experiment to study mechanisms of homogeneous and heterogeneous catalysts and guide the development of new and improved catalyst systems relevant to sustainable chemistry and energy technologies.

© 2018 The Authors. Published by Wiley-VCH Verlag GmbH & Co. KGaA

and/or void spaces accommodating the BASs also have a strong impact on their catalytic behavior.[27] The reactivity of BAS is directly related to the density, spatial arrangement and local environment of Al atoms in the zeolite framework. The unambiguous identification of the positions of framework Al and the associated BAS, and accordingly, understanding how the location of the site affects its acidity and catalytic properties remain an important challenge in zeolite catalysis.

Distribution, Mobility, and Property-Activity Relationships for Zeolite Brønsted Acid Sites

The location of Al in zeolites has been studied by the combination of ^{27}Al NMR experiments and DFT calculations.[28] It is generally recognized that the occupation of the framework T-site (T stands for the tetrahedral lattice Si or Al atom) by Al is not random or controlled by intrinsic chemistry of the system, but rather governed by the specifics of a particular synthetic method and conditions. The first quantitative analysis of the distribution of Al in a relatively simple scolecite zeolite containing only two distinct T sites was carried out using the X-ray standing wave (XSW) technique.[29] Subsequently, the Al occupancy in a more complex H-BEA material was investigated by a combination of X-ray absorption and ^{27}Al NMR spectroscopies, supported by DFT based aiMD simulations.[30] The results of this multi-technique analysis demonstrated that the distribution of Al is determined by kinetic factors during the synthesis rather than the thermodynamic stability of T-site substitutions. It was shown that the Al distribution can markedly vary depending on the Si/Al ratio (Figure 1).

DFT calculations were used to study the sitting location of framework Al and the distribution of BASs in an H-form of mordenite (MOR) zeolite.[31] A correlation between the T–O–T angle and the protonation energy has been established. It was concluded that sites with larger T–O–T angles are more tolerant to lattice distortions due to replacement of lattice Si with Al giving rise a lower O–H frequency and higher Brønsted acidity and reactivity.[31–32] On the other hand, a more recent computational study by Jones and Iglesia analyzed the ensemble-averaged deprotonation energies of six zeolites including MFI (silicalite-1), BEA (beta), FER (ferrierite), MOR (mordenite), CHA (chabazite) and FAU (faujasite) and concluded that no systematic correlations could be established between the Brønsted acidity and the length of O–H bonds and the Si–O–Al bond angles in those zeolites.[33]

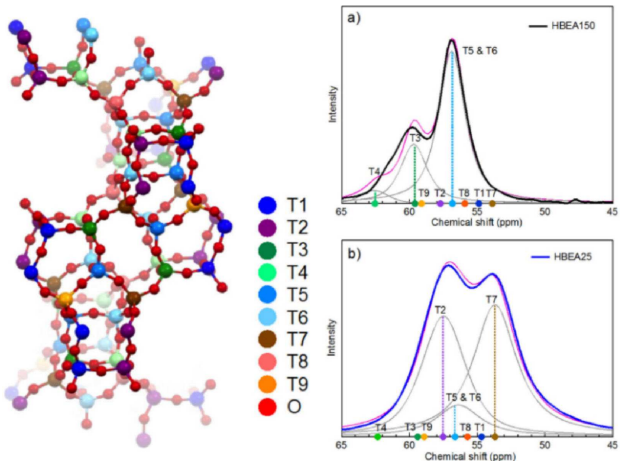

Figure 1. The locations of the nine different T-sites in HBEA, and calculated ^{27}Al MAS NMR chemical shifts for the tetrahedral Al based on the DFT optimized T-site structures for the measured HBEA150 (a) and HBEA25 (b). DFT NMR peak intensity is based on fitting results.[30] Reprinted with permission from *J. Am. Chem. Soc.*, 2014, 136, 8296. Copyright 2014 American Chemical Society.

Bell and co-workers carried out a combined experimental and computational study where the effect of the chemical composition of H-ZSM-5 zeolite on the spatial localization of BAS was investigated in detail.[34] It was demonstrated that the increase of lattice Al contents is accompanied by the increased concentration of BASs at the intersections of straight and sinusoidal channels. This leads to the preference of dehydrogenation of n-butane than the cracking, because of the better stabilization of the bulkier transition state structure of the dehydration path at the intersection. This study highlights the dual role of the intrinsic acidity of the BAS and confinement in the micropores for the reactivity of zeolite materials.[34] Furthermore, the sitting of Al atoms and their spatial proximity can affect the adsorption selectivity for central C–C bonds relative to terminal bonds of n-alkanes that has a direct impact on the selectivity of subsequent transformations. In particular, neighboring Al atoms can synergistically enhance the adsorption of central C–C bonds. Such a proximity effect is also reflected in the more pronounced polarization of adsorbed acetone and alkanes in zeolites.[35]

The intrinsic mobility (rate of proton hopping) of the protons inside zeolite depends on the lattice basicity that is, in turn, a direct function of the chemical composition and the local structure of the zeolite.[36] It was measured that the average activation barriers for proton hopping among bridging oxygens around the first-coordination sphere of Al atom are 45, 54, and 61 kJ/mol for H-ZSM-5, H-MOR and H–Y zeolites, respectively. This indicates a higher proton delocalization in H-ZSM-5, which was found to correlate with the Brønsted acidity of those zeolites (H-ZSM-5 > H-MOR ≫ H–Y).[37] Depending on the selected model and method, DFT calculations estimated the barriers of proton hopping in MCM-22 are in the range from 23 to 133 kJ/mol.[38] The rate and favorability of proton hoping can be greatly enhanced in the presence of water near the BAS[39] and they commonly show a strong temperature-dependence. The temperature dependence of the line width of ^{1}H MAS NMR reveals that the mobility of proton in H-ZSM-5 can be initiated at temperature as low as 370 K despite no proton mobility was detected at 298 K.[40] The computed hoping barrier corrected by tunneling effect for H–Y zeolite pointed to a similar temperature of 368 K at which the hoping is triggered.[41] High-temperature FTIR spectroscopic study complemented by DFT calculations identified two types of mobility of the acidic OH groups encountered at two different temperature ranges. Liberated protons may move across the four oxygens bound to the lattice Al at lower temperatures (< 573 K), while at high

© 2018 The Authors. Published by Wiley-VCH Verlag GmbH & Co. KGaA

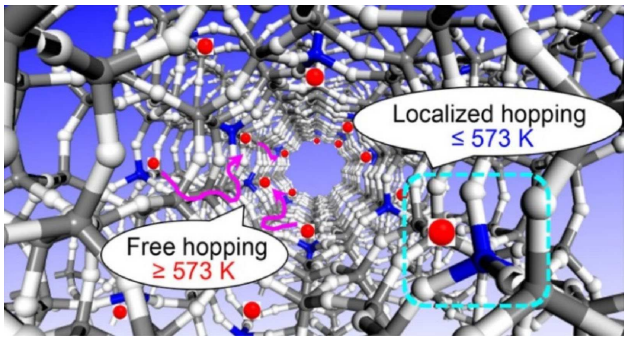

Figure 2. Liberated protons move across four lattice oxygen atoms around the Al site at lower temperatures (≤ 573 K) and in wider regions over the framework at higher temperatures.[42] Reprinted with permission from *J. Phys. Chem. C.*, 2017, 121, 25411. Copyright 2017 American Chemical Society.

temperatures, the protons may travel in wider regions over the framework (Figure 2).[42]

For the reactions in solution, the zeolite acidity can be influenced by the secondary solvent-induced effects.[43] Termath et al. simulated water adsorption in the microporous H-SAPO-34 zeolite in the 300–400 K range by aiMD and found that both water and hydronium ion can coexist in the pores of H-SAPO-34 loaded with water.[44] This is in line with the experimental low-temperature neutron diffraction data.[45] The hydrogen bonding between a single water molecule and an isolated BAS is not strong enough to form a H_3O^+ hydronium, but these can be stabilized upon more extensive solvation to form hydronium clusters $H_3O^+(H_2O)_2$. It was also shown that the ion-paired hydronium clusters can expel water molecules to form zeolite BAS upon the decrease of the temperature.[46] In addition, the solvation effect and proton transport efficiency can be induced by dispersion interactions as exemplified by the combined NMR and DFT study of trimethylphosphine oxide (TMPO) adsorption in H-ZSM-5 zeolite.[47] The proton solvation equilibrium depends on the topology and composition of the zeolite lattice which provide different spatial confinement effects and different adsorption structures. The specific location and structural environment of BAS in zeolite pores as well as the concentration and proton affinity of confined solvent molecules all influence the extend of deprotonation. Therefore, acidic zeolite can be viewed as strong acids while providing additional advantages of high selectivity originating from the specific sterics of zeolite micropores. The solvent effects on zeolite BAS can influence the preferred reaction mechanism by stabilizing the specific protonated reaction intermediate.[48]

The BAS can also be solvated by the reactant in the course of the reactions giving rise to the enhanced proton mobility in zeolite pores. The methylation of benzene with methanol in H-ZSM-5 was studied by aiMD and nonequilibrium metadynamics, which allowed exploring several alternative reaction pathways while accounting for the flexibility of the zeolite framework and the mobility of the reagents inside the pores. It was shown that at high methanol loadings, stable and mobile protonated methanol clusters are formed resulting in several orientations of the methanol-benzene pair with respect to the lattice. In addition, methylation can occur at remote locations relative to the original BAS suggesting that the exact Al localization may be less important for the reactivity than conventionally assumed.[49] Further results indicate that the van der Waals interactions between the hydrocarbon and the zeolite can considerably stabilize the transition states resulting in the reduction of specific activation barriers while the stronger acid site significantly decreased the barriers for all the reaction steps.[50]

Schneider and co-workers carried a combined experimental and theoretical study on the mechanisms of the selective catalytic reduction (SCR) of NO/NO_2 by an H-SSZ-13 zeolite.[51] A detailed kinetic model was constructed based on the results of DFT, metadynamics and aiMD calculations. Two distinct kinetic regimes were identified at temperatures between 473 and 673 K corresponding to the mechanism involving physisorbed NH_3 and free and mobile NH_4^+ cations inside the zeolite pores (Figure 3). The adsorption of NH_3 over the BAS in CHA zeolite also favors the NH_4^+-zeolite$^-$ motif and the comparison of the results obtained at different levels of DFT theory using cluster and periodic models imply the high potential of the hybrid QM/MM methods to deliver high accuracy along with the reduced computational time.[52]

A widely employed approach to evaluate acid strengths in heterogeneous catalysis relies on adsorption of weakly basic

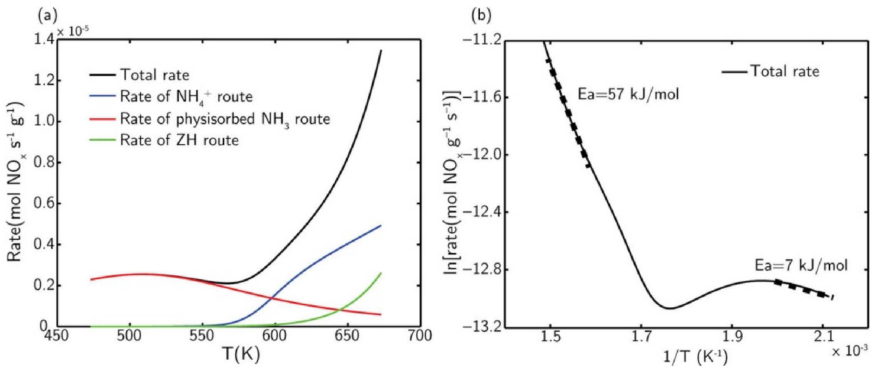

Figure 3. (a) Computed total and individual sites rates of NOx SCR per gram H-SSZ13 catalyst vs temperature. (b) Arrhenius plot of total rate of NOx SCR. Rates were computed at 180 ppm of NO and NO_2 and 360 ppm of NH_3.[51] Reprinted with permission from *ACS Catal.*, 2017, 7, 5087. Copyright 2017 American Chemical Society.

© 2018 The Authors. Published by Wiley-VCH Verlag GmbH & Co. KGaA

molecular probes.[53] The red shift of the stretching frequency of acidic OH group upon the interaction with the basic probe is commonly correlated to the BAS strength, although other factors may also affect the observed frequency.[54] The decrease in lattice Al concentration in FAU-type zeolites results in higher BAS strength up to Si/Al values of ca. 45 when the acidity effectively levels off.[55]

The intrinsic acidity of zeolite BAS can be approximated by the deprotonation energy (DPE) that is the dissociation energy of the O–H bond. The linear relationship between the DPE and the turnover rates of alcohol dehydration and skeletal isomerization of alkenes on zeolites has been reported by Iglesia and co-workers.[56] The correlations between the apparent activation barrier of alkane cracking and the DPE were also reported for a series of H–Y zeolites.[57] However, more recent studies suggest that DPE cannot be used as a universal descriptor to capture the catalytic activity of solid acids, because other factors, such as the interaction of the cationic transition state with the conjugate anionic zeolite framework, also affect the catalyst reactivity.[58]

The strength of the acid sites can also be directly correlated to the heat of adsorption of the basic probe. Borges and co-workers used DFT calculations to demonstrate that the activation barrier of n-hexane protolytic cracking scales linearly with the adsorption enthalpy of ammonia over the BAS in H-ZSM-5 zeolites, which was in line with the experimental results.[59] Adsorption energy of ammonia was proposed as a suitable descriptor for constructing scaling laws to estimate activation barriers of elementary steps as well as the reaction rate of alkene methylation.[58a,60] It is important to note that such (single) property-activity scaling relations constructed for one zeolite type may not necessarily hold for other topologies because of the different van der Waals interactions and geometric constraints imposed by zeolite pores with different topologies.[61]

Confinement Effects in Zeolite Catalysis

The location of BASs inside the micropores strongly affects their reactivity. The varied spatial constraints at different zeolite sites may affect the stability of reactants and transition state affecting thus the overall free energy profile of the reaction and the observed reactivity.[62] The effect of confinement in zeolite micropores on the selectivity of methanol conversion was clearly illustrated by the comparison of two series of H-ZSM-5 zeolites with the sinusoidal (T-HZ) and straight (S-HZ) channels enriched with Al. The two materials showed similar intrinsic acidity, morphology and textural properties. Yet, the conversion of methanol by T-HZ gives higher selectivity to ethylene and aromatics than by S-HZ, which, in turn, provides higher selectivity to propene and higher olefins.[63] Similarly, the crucial role of the pore size and shape for the methanol to olefin (MTO) conversion was revealed by DFT calculations.[64] Lercher and co-workers employed a combination of DFT and aiMD simulations to investigate the aqueous propanol dehydration over H-ZSM-5 zeolite.[65] The analysis of the dehydration activity of the hydronium ion in MFI, BEA and FAU zeolites revealed that the catalytic activity can be tuned by altering the compensation between enthalpy and entropy induced by microporous environment via either enhancement of the interaction between hydronium ions and alcohol reactant or offset of the higher activation enthalpies by more positive activation entropies.[66]

Bucko et al computationally studied the reaction dynamics of proton exchange, alkane cracking and dehydrogenation reactions by acidic zeolites.[67] The computational results emphasize the non-negligible entropic contributions in these hydrocarbon conversion reactions.[68] The aiMD simulation of monomolecular propane cracking showed that the mobility of the reactant is considerably enhanced and the adsorption energy is reduced at elevated temperature due to the weak interaction of the adsorbed molecule with the BASs. Therefore, only a fraction of reactant complex is formed sufficiently close to the acid site to initiate the protonation reaction. By using the transition path sampling (TPS) method it was demonstrated that the protonation reaction preferentially takes place at the terminal methylene group whereas the direct activation of the internal C–C bonds occurs with a much lower possibility.[69] Tranca et al investigated the temperature dependence of enthalpy, entropy, Gibbs free energy as well as the adsorption equilibrium constant of short chain alkanes in H-ZSM-5 zeolite by Monte Carlo (MC) simulations. They found that both enthalpy and entropy contributions become less negative with increasing temperature. This is especially the case for longer chain alkanes. The adsorption free energy slope and the adsorption equilibrium constant have observable deviations from the ones obtained from the experimental data under the temperature independent assumption (Figure 4).[70] Bell and co-authors analyzed the product distribution of n-pentane cracking reaction by using quasiclassical trajectory (QCT) approach based on molecular dynamics simulations. It has been shown that the metastable carbocationic species stabilized by the electrostatic interaction with zeolite framework can be very flexible and present with many iso-stable configurations. These configurations may lead to diverse product distributions (Figure 5).[71] Later on, the authors compared the thermodynamic properties and the reaction pathways of n-hexane cracking in acidic ZSM-5 and Y zeolites. It was concluded that different pore size leads to varied interaction strength between the reactant and zeolites, but the kinetics of cracking is independent of the acid strength. The reaction selectivity analysis evidenced that both reaction dynamics of metastable intermediates and reaction barriers determine the product selectivity.[72]

A systematic investigation was carried out on the adsorption thermodynamics and intrinsic kinetics of alkane monomolecular cracking and dehydrogenation in zeolites with different pore size and channel topology by a combination of experiment, QM/MM, and configurational-bias Monte Carlo (CBMC) simulation.[34,73] It was found that the intrinsic activation energies of cracking and dehydrogenation are determined by the locations of the BASs as well as the topological properties of the zeolite framework.[73a] The adsorption equilibrium constant ($K_{ads\text{-}H+}$) at 773 K depends strongly on the entropy changes ($\Delta S_{ads\text{-}H+}$) but not on the changes in adsorption enthalpy ($\Delta H_{ads\text{-}H+}$). Therefore, the adsorption in more confined zeolites has lower value of $K_{ads\text{-}H+}$.[73b] This conclusion is not

© 2018 The Authors. Published by Wiley-VCH Verlag GmbH & Co. KGaA

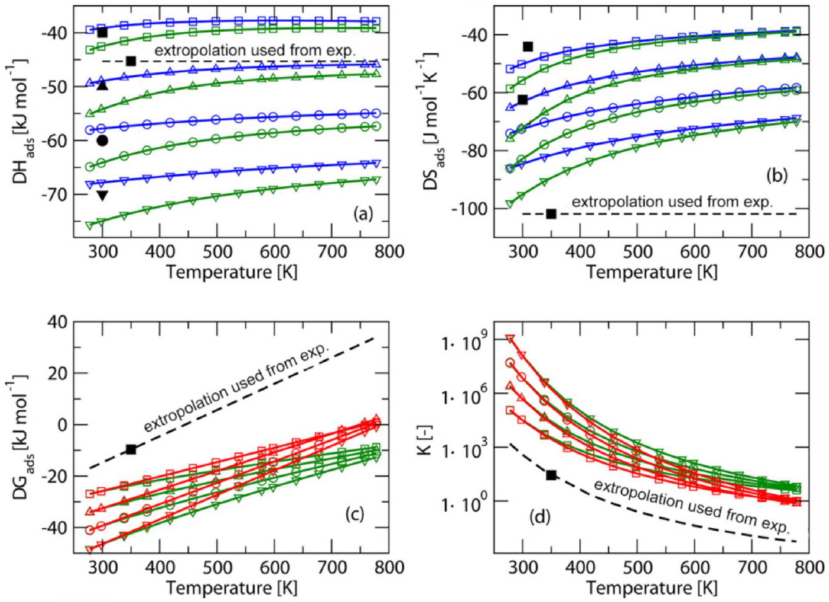

Figure 4. Parameters related to the adsorption of propane (□), n-butane (Δ), n-pentane (o), and n-hexane (▽) in silicalite (blue) and H-ZSM-5 (red). The open symbols represent the MC simulation results, the filled symbols represent experimental data. (a) Heat of adsorption as function of temperature. (b) Entropy of adsorption as function of temperature. (c) Free energy of adsorption as function of temperature. (d) Adsorption equilibrium constant as a function of temperature.[70] Reprinted with permission from *J. Phys. Chem. C.*, 2012, 116, 23408. Copyright 2012 American Chemical Society.

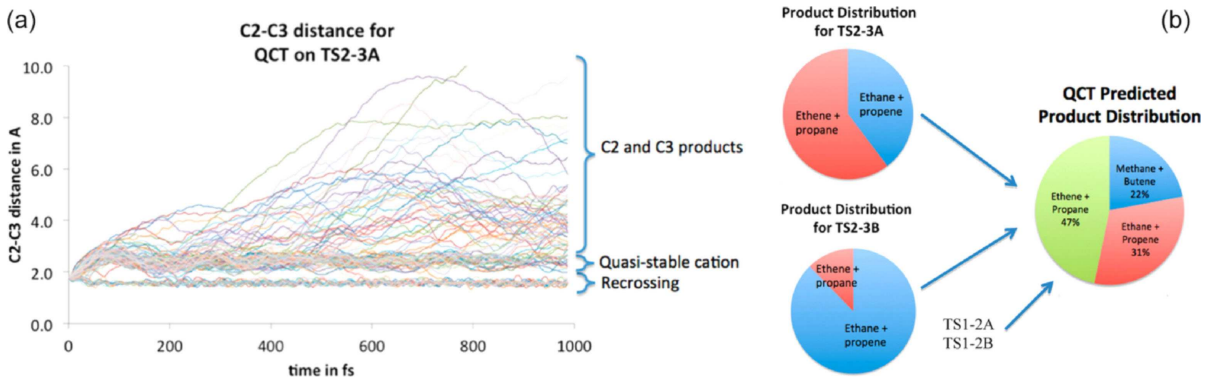

Figure 5. (a) The C2–C3 distance of n-pentane cracking transition state to C2 and C3 products as a function of time and (b) final product distributions predicted at 773 K by the QCT simulations.[71] Reprinted with permission from *J. Am. Chem. Soc.*, 2012, 134, 19468. Copyright 2012 American Chemical Society.

consistent with previous reports, which emphasized that the adsorption equilibrium constant is determined by adsorption enthalpy and generally is the cause for different apparent rate constants (k_{app}) obtained for n-alkane cracking in MFI, MOR, BEA and FAU zeolites.[74] Furthermore, the intrinsic activation enthalpy and entropy deduced from measured activation parameters and simulated adsorption thermodynamics indicate that both parameters are zeolite structure dependent. This finding also strongly deviates from the conclusions of earlier works.[62,75]

Effect of Extraframework Lewis Acid

A practical approach to tuning the Brønsted acidity and enhancing the catalytic activity is to subject a low-silica zeolite catalyst to hydrothermal and/or calcination treatments, which usually results in the removal of aluminum from the framework site and the formation of extraframework aluminum (EFAl) species.[76] For instance, steam-calcination of low-silica FAU-type zeolite (Si/Al < 3) results in a pronounced enhancement of its Brønsted acidity and overall performance in acid-catalyzed transformations.[7e] In part, this acidity enhancement is directly related to the reduction of the proton affinity of the more siliceous framework (i.e. having a higher framework Si/Al ratio). Besides, it was noted that the migration of Al ions from its lattice position and the generation of Lewis acidic EFAl species

© 2018 The Authors. Published by Wiley-VCH Verlag GmbH & Co. KGaA

may also have an impact on the acidity of the steam-calcined zeolite materials.[77] Experimental catalytic tests revealed the correlation between the increase in the rate of monomolecular propane cracking and the presence of cationic EFAl species inside the pores of FAU-type zeolites. It was proposed that the enhanced catalytic performance is related to the synergistic effect between the BAS and its adjacent Lewis acidic EFAl species.[78] An alternative mechanistic proposal rationalizing this phenomenon implies that the presence of bulkier EFAL complexes in the zeolite micropores bring about the geometrical changes in the zeolite confinement space, resulting in the more efficient non-covalent stabilization of the reaction intermediates and transition states.[79]

Until recently, the mechanistic analysis on the nature of the EFAl in zeolites and their role in catalytic processes was complicated by the apparent lack of the direct structural information on EFAl complexes in zeolite pores. Earlier DFT studies on the structure and promoting effect of EFAl complexes were carried out in the framework of the cluster modelling approach and considered only rather small mononuclear single-site EFAl species.[19a] The coordination and stability of six types of mononuclear cationic EFAls with varied chemical composition and charge were investigated by Mota and co-workers using a T6 zeolite cluster model representing a part of the stabilizing zeolite lattice. Zheng et al successfully verified the presence and plausible location of the mononuclear tri-coordinated Al^{3+} EFAl in dealuminated HY zeolite very recently by the combination of DFT and ^{31}P solid-state NMR.[80] It was computationally demonstrated that the strength of the BAS can be enhanced in the presence of a bivalent $[Al(OH)]^{2+}$ cation that was proposed as the most probable EFAL complex.[81] The combined solid-state NMR and DFT study by Deng and co-workers provided further evidences on the importance of the synergy between BAS and EFAl for the activity enhancement of acidic zeolites.[78b] It was proposed that mononuclear $Al(OH)_3$ and $Al(OH)^{2+}$ are the preferred EFAL motifs and they can be accommodated at cation sites both in the supercage and sodalite cage of steam-calcined HY zeolite. The increased Brønsted acidity was attributed to the additional stabilization of the negative charge of zeolite framework provided by the cationic EFAl species. The interaction of EFAl with the lattice oxygen atoms weakens the adjacent O–H bonds, which, in turn, leads to the increased acidity of the associated BAS (Scheme 1). Other researchers proposed that that the polarization of an OH group by the vicinal multinuclear EFAL clusters may also contribute to the increased acidity of BAS.[82]

Recently, periodic DFT calculations combined with aiTA analysis revealed that under the conditions of thermochemical zeolite activation, there is a clear thermodynamic preference for the formation of multinuclear multiply-charged $[Al_3O_4H_3]^{4+}$ EFAl cationic clusters inside the small FAU sodalite cages. The stabilization in the sodalite cage limits the accessibility of the EFAl complex from any reactant that is in line with the hypothesis on indirect interaction between BAS and EFAl species.[22b,83] Computations reveal a profound stabilizing effect of EFAl on both the transition state and the product of the protonation reaction. This finding provides a clear evidence that cationic EFAl species are able to indirectly impact the Brønsted acidity and catalytic reactivity by improving the efficiency of the compensation for the charge of the anionic zeolite lattice during the proton transfer reaction. A similar mechanism of acidity enhancement has been proposed to rationalize the enhanced reactivity of lanthanum-exchanged FAU zeolite (La-FAU) in alkylation process. La species also tend to aggregate into multinuclear cationic La-oxo/hydroxo clusters inside the sodalite cages.[84] The increased acidity of BAS due to cationic La complexes is the key to sustaining the system within the alkylation cycle and, at the same time, inhibiting the deactivation reaction channels.

Theoretical studies indicate that the catalytic role of EFAl, mechanism of the acidity enhancement and the way these effects are manifested in the actual experiment may substantially vary depending not only on the nature of the stabilizing zeolite matrix but also on the actual catalytic process being considered. DFT calculations suggest that the presence of EFAl in FAU zeolite may give rise to substantial alternations of the activity-acidity relationships established using different probe reactions.[55] Whereas a consistent correlation between the barrier of monomolecular propane cracking and the BAS acidity reflected in the adsorption energies of different base could be established for a range of dealuminated EFAl-free and EFAl-containing faujasite models, a linear relation did not hold for the H/D exchange in benzene. In the presence of EFAl, the H/D exchange reaction mechanism changes from a one-step concerted reaction to a two-step process so that the transition states for the different types of zeolite systems were not related anymore.

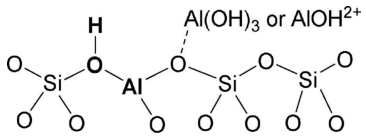

Scheme 1. Brønsted-Lewis acid synergy between a model mononuclear EFAl and BAS.

Lewis Acidity of Zeolites

Besides having an impact on the Brønsted acidity, Lewis acidity itself is a key property defining the broad scope of catalytic applications of zeolite materials. The specific Lewis acidic sites can be introduced into the zeolite matrices either by modifying the lattice composition or by stabilizing reactive complexes at zeolite cation sites.[85,86] The isomorphous substitution of framework Si atoms by other tetravalent metal cations such as Ti^{4+}, Sn^{4+}, Zr^{4+} gives rise to Lewis acidic species embedded in the siliceous zeolite framework (Scheme 2a). The catalytic properties of zeolites featuring this type of active sites are associated with the presence of highly-dispersed and well-defined single-site LAS. An alternative and more general approach to zeolite modification is based on the exchange of the charge-compensating protons or alkali cations in zeolites by other cationic metal-containing species resulting in extraframework LASs stabilized by the lattice oxygens from anionic $[AlO_2]^-$ units (Scheme 2b). The structure and catalytic properties of such LAS

© 2018 The Authors. Published by Wiley-VCH Verlag GmbH & Co. KGaA

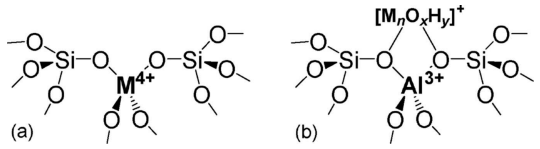

Scheme 2. (a) Framework and (b) extraframework Lewis acid sites in zeolites.

are influenced by the spatial distribution of Al in the zeolite lattice as well as by the geometry of the cation site and the basicity of the lattice oxygen ions acting as the ligands stabilizing the cationic species.

Framework Lewis Acid Sites

The isomorphous substitution of lattice silicons with such tetravalent cations as Ti^{4+}, Zr^{4+} and Sn^{4+} that do not bring about local charge disbalance is one of the most popular and well-studied approaches to generation Lewis acid sites in zeolites. Such materials have been found to be particularly active in the catalytic activation of carbonyl moieties of organic substrates.[86] Zeolites modified with Sn find numerous applications as catalysts for the selective conversion of carbohydrate fraction of biomass. The high Lewis acidity of Sn sites embedded in the hydrophobic high-silica zeolite environment renders such materials promising water-tolerant Lewis acid catalysts for such biomass conversion steps as the carbohydrate isomerization, epimerization and aldol condensation reactions.[14c,87]

Lattice-substituted zeolites are often referred to as the single-site heterogeneous catalysts that is the materials featuring highly uniform and dispersed speciation of the reactive sites. However, recent experimental studies provide evidence of a substantial active site heterogeneity in such materials.[88] Wolf et al employed dynamic nuclear polarization (DNP) ^{119}Sn solid-state NMR spectroscopy to investigate a series of highly active Sn-Beta materials prepared by different research groups. The study revealed that in spite of the similar catalytic behavior, the Sn speciation in different catalyst samples was characterized by drastically different spectral features.[89] Such a site heterogeneity may be attributed to the varied degree of chemical modification of the heteroatoms (i.e. partial hydrolysis) caused by the differences in the synthesis procedures and/or the variations in the local environment around the heteroatoms.

The local coordination environment of LAS is determined by the topological properties of the zeolite matrix and the location of the guest atom in it. The relation between the distribution, stability and reactivity of framework LAS has been a subject of experimental and theoretical works.[90] The distribution of Ti atom in the framework of TS-1 zeolite has been investigated and it was concluded that the preferred sitting of Ti atoms in the lattice is not controlled by the thermodynamic stability of the substitutions in the final material but rather by other kinetic and thermodynamic factors encountered at the stage of the zeolite growth.[91] Pal and co-workers used periodic DFT calculations to compare the location, Lewis acidity and hydrophilicity of both Sn- and Ti- sites in BEA zeolite. Lattice T1 and T2 sites were identified as the most favorable sitting locations for both systems. Computations predicted that the higher Lewis acidity of Sn substitutions was achieved at the expense of their lower intrinsic stability compared to Ti-modified counterparts.[92] These findings were consistent with the results of a periodic DFT study by Yang et al, who investigated the sitting and reactivity of Ti, Sn and Zr in BEA zeolite and demonstrated a strong influence of the location of the guest atom on its Lewis acidity.[93] The variations in the Lewis acidity were attributed to the differences in the accessibility of the lattice sites. This study also evaluated computationally the possibility of forming paired Lewis acid sites capable of concert substrate activation. Only in the case of Sn-BEA, the formation of such cooperative sites was predicted to be thermodynamically favored.

The chemical heterogeneity of framework Lewis sites is directly related to their intrinsically high reactivity. In addition to the perfect tetrahedral four-fold coordinated T sites in the framework (so called "closed site"), the heteroatoms can also take form of the partially hydrolyzed species (so called "open site"), in which one or several links with the silicious framework has been cleaved upon the reaction with water (Scheme 3).

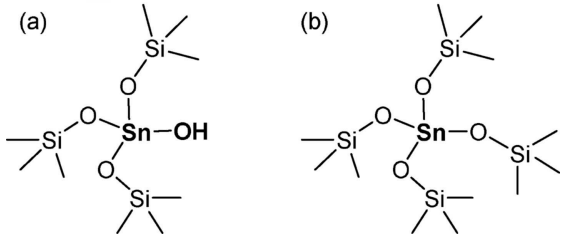

Scheme 3. Schematic representation of the open and close Sn sites

Such partially hydrolyzed SnOH species have been proposed as the catalytically active sites in Sn-BEA zeolite.[88e,94] Similar lattice defects featuring TiOH and adjacent silanol in TS-1 appear to be more reactive than their closed Ti^{4+} counterparts in selective oxidation and sugar isomerization reactions.[94–95] The location and structural properties of open Sn sites in Sn-Beta have been surveyed by comparing the relative energies of 144 distinct structures. [96] It was shown that SnOH has a preference for occupying the T9 and T1 lattice positions. Furthermore, computations show that the vicinal SnOH and SiOH moieties of the open site do not engage in hydrogen bonding. As a result, the Sn-open site SiOH group appears to be significantly more acidic than the silanol moieties at the external surface or within lattice defects. Furthermore, the heteroatoms may be extracted from the lattice to form extraframework species under the catalytic conditions contributing thus further to the active site heterogeneity of framework-modified zeolites.[97]

© 2018 The Authors. Published by Wiley-VCH Verlag GmbH & Co. KGaA

Extraframework Lewis Acid Sites

The anionic sites of the aluminosilicate lattice form a suitable ligand environment for the stabilization of metal cations and cationic ensembles providing thus a versatile path towards tailored reactivity of zeolite materials. The location and structure of the guest cationic species are sensitive to distribution of charge-compensating lattice $[AlO_2]^-$ anions. Basic electrostatic considerations suggest that for zeolite with high Si/Al ratios featuring very high dispersion of lattice aluminum, there should be a preference for the formation of EF complexes having $+1$ charge so that their charge-compensation through the direct interaction with the lattice ion could be established. The plausible configurations are such metal-oxo/metal-hydroxo complexes as $[MO]^+$, $[MOH]^+$, or $[M_nO_xH_y]^+$. For zeolite with low Si/Al ratio, the density of Al in the framework is high and so is the fraction of paired Al sites $(–Al–O(–Si–O–)_x–Al–, x<3)$. Such an increased local density of lattice negative changes enables the direct charge-compensation of multiply charged cationic species, which are not limited to single transition metal ions but can take form of a wide range of cationic complexes such as, for example, the EFAl and EF La species discussed in the previous section. The catalytic properties of the resulting materials will be determined by the structure of the EF species and also by the properties of the confined environment.[22b,98]

Self-Organization of Extraframework Cations

In principle, at low metal loading and for low-silica zeolites having a high density of paired lattice Al sites, the multivalent cationic metal-oxo(hydroxyl) complexes prefer to occupy the exchange sites where direct coordination bonds can be formed with a maximal number of the negatively-charged framework oxygen atoms of $[AlO_2]^-$ fragments. For materials with high Si/Al ratio, such cations can also potentially occupy energetically less favorable sites with fewer $[AlO_2]^-$ fragments in their first coordination sphere. To illustrate this phenomenon, let us consider high-silica Ga-modified zeolites as a representative example. Such materials are efficient catalysts for dehydrogenation and aromatization of different substrates including light alkanes and biomass-derived furanics.[99] Experimental studies revealed that the catalytic performance of well-defined Ga^+-containing zeolites can be enhanced by a stoichiometric treatment with N_2O, which supposedly gives rise to isolated $[GaO]^+$ gallyl cations.[100] This structural proposal was mainly based on the considerations of the low lattice Al density and the direct charge-compensation requirement, and it was supported by EXAFS data. However, no favorable reaction path for alkane dehydrogenation could be computationally established over single-site mononuclear species.[101]

To resolve this apparent discrepancy between theory and experiments, periodic DFT calculations on the structure of oxygenated Ga cations in a high-silica MOR model with a chemical composition resembling that of the practical catalyst was carried.[102] Figure 6 compares the computed stabilities of different isomeric Ga_2O_2 (that is two isolated $[GaO]^+$ ions and the products of their self-organization into binuclear clusters) in two selected high-silica MOR models with different spatial distribution of Al atoms. As to be expected from basic electrostatic considerations, calculations showed that the distribution of lattice aluminum had little impact on the stability of mononuclear Ga^+ and $[GaO]^+$ species, while the stabilities of the derived binuclear aggregates appear to be more sensitive to this factor. Nevertheless, the energy gain due to formation of the favorable coordination environment of the metal sites upon the self-organization of gallyl ions into binuclear $[Ga(\mu\text{-}O)_2Ga]^{2+}$ clusters compensated for the less favorable indirect charge-balancing mechanism.

These computational data provided a direct evidence that self-organization of gallyl moieties driven by coordination preference can offset the energy gain of the contact charge compensation, which suggest that the binuclear gallium-oxo clusters are the dominant species in high-silica zeolites. Such self-organization of oxygenated cations is not a unique property for Ga-zeolite system, but a general phenomenon for many different metal-containing species in zeolite. For example, the same coordination-driven structural reconstruction has also been verified for such system as Zn, Cu, Fe, Al and La modified ZSM-5 zeolites. The same tendency of aggregation of mononuclear metal-containing cationic species into binuclear or oligonuclear clusters has been rationalized by periodic DFT calculations.[103]

Structure, Location and Stability of Extraframework Cations

The determination of the structure and location of cationic metal sites is an important topic in zeolite catalysis.[104] DFT calculations provide practical means to simulating the entire periodic zeolite framework and exploring all hypothetic locations and structure-property relations of guest metal species at the atomic level. Fe/ZSM-5 is one of the most investigated zeolite catalysts because of its outstanding catalytic properties for such processes as N_2O decomposition, selective catalytic reduction of NO_x and hydrocarbon oxidation.[105] However, the structure and location of iron-containing extraframework (EF) cation sites in such catalysts are still debated. Fe/ZSM-5 can contain a wide range of species including isolated Fe^+/Fe^{3+} species, mono-, bi- or oligonuclear iron-oxo complexes, or iron oxide nanoclusters in zeolite micropores. The nature of these iron-containing species has been intensively discussed and different complexes have been proposed to be the active sites by both experimental and computational studies.[106]

Electronic structure DFT calculations provide the information on the intrinsic stability of the intrazeolite species under idealized model conditions representing a system at ultra-high vacuum and 0 K.[21] The impact of the environmental effects such as the finite partial pressures and temperature on the stability of intrazeolite ensembles during the catalyst activation or even the catalytic reaction can be accounted for by constrained ab initio thermodynamic (aiTD) method.[107] This approach allows directly comparing stabilities of molecular

© 2018 The Authors. Published by Wiley-VCH Verlag GmbH & Co. KGaA

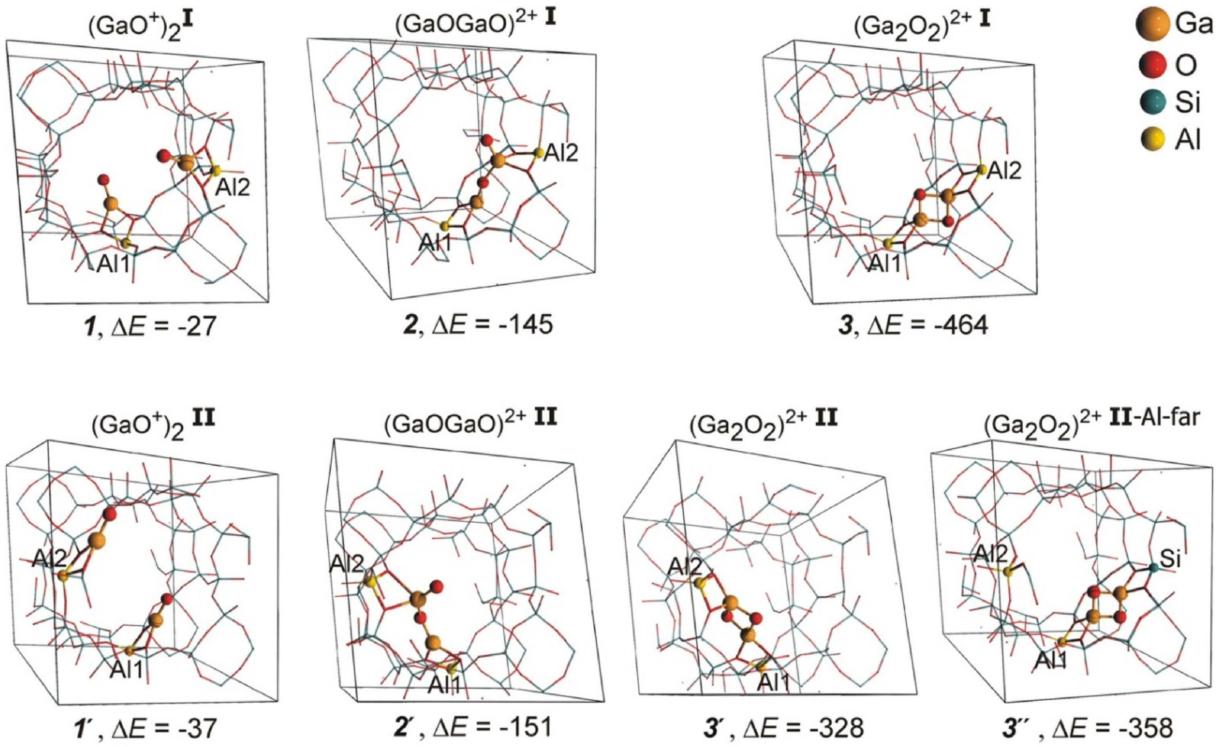

Figure 6. Optimized structures of $(GaO)_2$ isomers stabilized in mordenite models I (upper row) and II (bottom row). The ΔE values (kJ/mol) correspond to the reaction energy for the stoichiometric oxidation of two exchangeable Ga + cations with N_2O toward the respective $(GaO)_2$ isomer according to the reaction $2Ga + MOR + 2\ N_2O \rightarrow (GaO)_2 + 2MOR + 2\ N_2$.[102a] Reprinted with permission from *J. Catal.*, 2008, 255, 139. Copyright 2008 Elsevier.

ensembles with different chemical composition by considering formation Gibbs free energy in the framework of a generalized reaction equilibrium for a given system. For a given metal containing zeolite system, the formation Gibbs free energies for different metal-containing complexes can be defined assuming a single reference system, from which they all originate. Such a reference can be bulk or nanocluster metal oxide and a Brønsted acidic zeolite. Assuming a generalized zeolite activation process via high-temperature calcination treatment, one can write then a stoichiometric reaction connecting these precursors and the final metal-containing complex in zeolite [Equation (1)]:

$$\begin{aligned} &a(MO_x) + H_y/\text{Zeolite} \rightleftharpoons M_aO_bH_c/\text{Zeolite} + ((y-c)/2)\ H_2O \\ &+((ax-b)/2-(y-c)/4))\ O_2 \end{aligned} \tag{1}$$

Then the formation Gibbs free energy of a particular EF metal-containing complex can be computed as [Equation (2)]:

$$\begin{aligned} \Delta G(T,p) = {} & G_{M_aO_bH_c/\text{Zeolite}} + ((y-c)/2)\ G_{H_2O} \\ &+((ax-b)/2-(y-c)/4))\ G_{O_2} - G_{H_y/\text{Zeolite}} - a^*G_{MO_x} \end{aligned} \tag{2}$$

Where $G_{M_aO_bH_c/\text{Zeolite}}$ and $G_{H_y/\text{Zeolite}}$ are the Gibbs free energies of zeolite containing a metal-oxo(hydroxyl) complex and the parent Brønsted acidic zeolite. G_{H_2O}, G_{O_2} and G_{MO_x} are the Gibbs free energies of gaseous water, oxygen and the reference bulk metal oxide, respectively. The factor *a* denotes the nuclearity of the EF complex formed. Here, the Gibbs free energies of solid zeolite models are approximated with DFT-computed electronic energies ($E_{M_aO_bH_c/\text{Zeolite}}$ and $E_{H_y/\text{Zeolite}}$) because the finite temperature and pressure have only negligible influences on the changes of enthalpy and entropy of solids. The Gibbs free energies for the gas-phase components of water and oxygen are calculated using their electronic energies and chemical potential differences including all enthalpy and entropic contributions related to temperature and pressure. The formation free energy takes therefore a form of [Equation (3)]:

$$\begin{aligned} \Delta G(T,p) = {} & E_{M_aO_bH_c/\text{Zeolite}} + ((y-c)/2)\ E_{H_2O} \\ &+(ax-b)/2-(y-c)/4)\ E_{O_2} - E_{H_y/\text{Zeolite}} \\ &- a^*E_{MO_x} + ((y-c)/2)\ \Delta\mu_{H_2O}(T,p) + \\ &((ax-b)/2-(y-c)/4))\ \Delta\mu_{O_2}(T,p) \end{aligned} \tag{3}$$

Then the chemical potential differences ($\Delta\mu_i$) are defined in Equation (4) and (5) as

$$\Delta\mu_{H_2O}(T,p) = \Delta\mu_{H_2O}(T,p^0) + RTln\left(p_{H_2O}/p^0\right) \tag{4}$$

$$\Delta\mu_{O_2}(T,p) = \Delta\mu_{O_2}(T,p^0) + RTln\left(p_{O_2}/p^0\right) \tag{5}$$

Thus, we are now able to express the formation Gibbs free energies of different EF metal-containing species as the

© 2018 The Authors. Published by Wiley-VCH Verlag GmbH & Co. KGaA

functions of the chemical potentials of gas-phase components, which are, in turn, directly related to the respective temperature and their partial pressures in the system. It is important to note that this approach only considers the thermodynamic stability of the chemical systems, while the kinetic factors as well as diffusion and mass transfer effects accompanying their interconversions are ignored.

The stabilities of various iron-containing complexes in Fe/ZSM-5 zeolite under the conditions of catalyst activation have been studied using aiTA method.[22a] Three types of species have been identified as the most stable in the given range of selected chemical potentials of water and oxygen (Figure 7). The binuclear

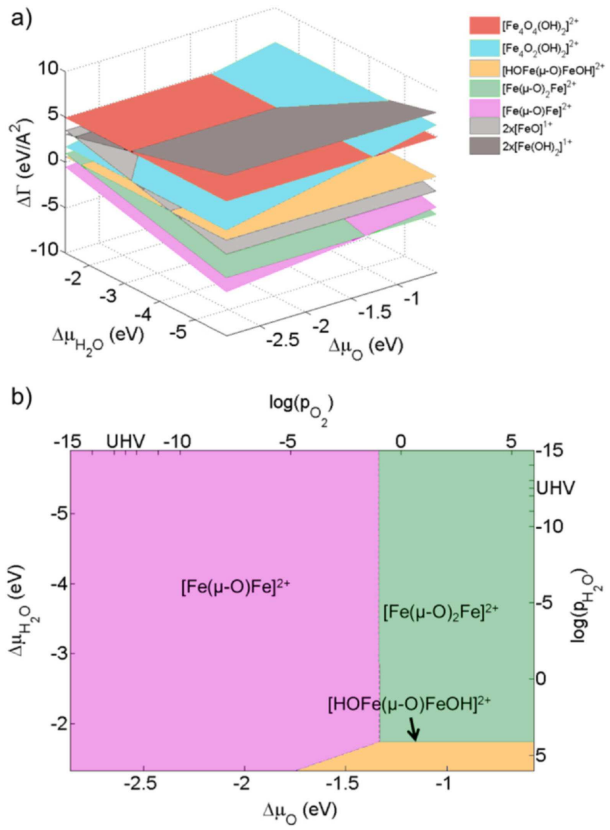

Figure 7. (a) Formation Gibbs free energy of $Fe_xO_mH_n$ in ZSM-5 as a function of oxygen chemical potential ($\Delta\mu_O$) and water chemical potential ($\Delta\mu_{H2O}$). (b) $\Delta\mu_O$ and $\Delta\mu_{H2O}$ are translated into pressure scales at T = 1100 K.[22a] Reprinted with permission from *J. Phys. Chem. C*, 2013, 117, 413. Copyright 2013 American Chemical Society.

EF $[Fe(\mu\text{-}O)Fe]^{2+}$ complex is the most stable species at low O_2 partial pressure (p_{O2}) and water-free condition, while at increasing p_{O2} it is oxidized to $[Fe(\mu\text{-}O)_2Fe]^{2+}$. In the presence of water, the hydroxylated $[HOFe(\mu\text{-}O)Fe]OH^{2+}$ cluster becomes the preferred EF cluster. All other complexes were found to represent metastable phases with higher formation Gibbs free energies compared to bulk iron oxide, and therefore their formation is highly unlikely in the activated catalyst. This method has also been successfully employed to study the speciation of EF Cu sites in Cu/ZSM-5[108] and Cu/MOR zeolite,[109] the structure of EFAl species in steam-calcined FAU zeolites,[22b] and the Cu-containing species in SSZ-13 zeolite under the condition of SCR of NO_x with NH_3[110] as well as porphyrin-supported copper oxide nanoclusters in oxidative atmosphere.[111]

Structure-Reactivity Relationships

High-silica zeolites modified with copper and iron are active catalysts for the selective conversion of methane to methanol at low temperature.[112] Many experimental and theoretical studies have been reported in the last decade aiming at understanding the nature and function of the active sites in these systems and establishing predictive structure-activity relations that could serve as a basis for the development of improved catalyst systems for selective methane oxidation.[12,112-114]

DFT calculations proposed that the spin-density on the reactive bridging EF oxygen centers of the active copper clusters is the important parameter for the facile activation of C–H bonds in methane. The radical nature of the reactive oxygen center was proposed to facilitate the homolytic C–H cleavage via a radical-like transition state to produce a CH_3 radical and a hydroxylated EF cluster.[108,116] Yoshizawa et al carried out DFT calculations to compare reactivity of $[Cu_2(\mu\text{-}O)]^{2+}$ and $[Cu_3(\mu\text{-}O)_3]^{2+}$ in MOR and MAZ zeolites and showed that water co-feeding can promote the oxidation process by facilitating the desorption of methanol from the active site, while it is unlikely that water can be act as the oxidizing agent to regenerate the active site with a concomitant formation of H_2.[117] These computational insights contrast the mechanism recently proposed by Sushkevich et al.[118] The computational studies reported so far indicate that despite differences in intrisic reactivity, Cu-oxo and Cu-hydroxo species with varied nuclearity can all contribute to the activity in selective methane oxidation by zeolites.[117–119] In addition to multinuclear clusters, mononuclear $[CuOH]^+$ species have also been considered as the potential active sites, although their role in the catalytic process remains controversial. Oord et al observed a correlation between the increase in methanol productivity and the intensity of the FTIR band due to $[CuOH]^+$ species.[120] These findings are in line with the results of DFT calculations by Kulkarni et al evidencing a pronounced reactivity of such sites toward CH_4.[121] On the other hand, earlier reports indicated that the involvement of $[CuOH]^+$ in methane oxidation over Cu/CHA is unlikely as followed from the critical examination of the reported catalytic and spectroscopic evidences.[112d,122] Such mononuclear Cu species were also found inactive in Cu/MOR.[123]

Schoonheydt, Sels, Solomon and co-workers combined a wide range of characterization techniques such as UV-Vis spectroscopy with site-selective magnetic circular dichroism (MCD) spectroscopy complemented by DFT calculations to identify the nature of methane oxidation sites in Fe/ZSM-5 catalyst.[115,124] It was shows that reactive α-Fe is a mononuclear Fe^{2+} cation in high-spin electronic configuration located in a six-membered ring featured with a square-planar geometry coordinated by four framework oxygen atoms. The α-O is its oxidative counterpart of a mononuclear $[FeO]^{2+}$ species, whose exceptional reactivity towards methane C–H bond activation is

© 2018 The Authors. Published by Wiley-VCH Verlag GmbH & Co. KGaA

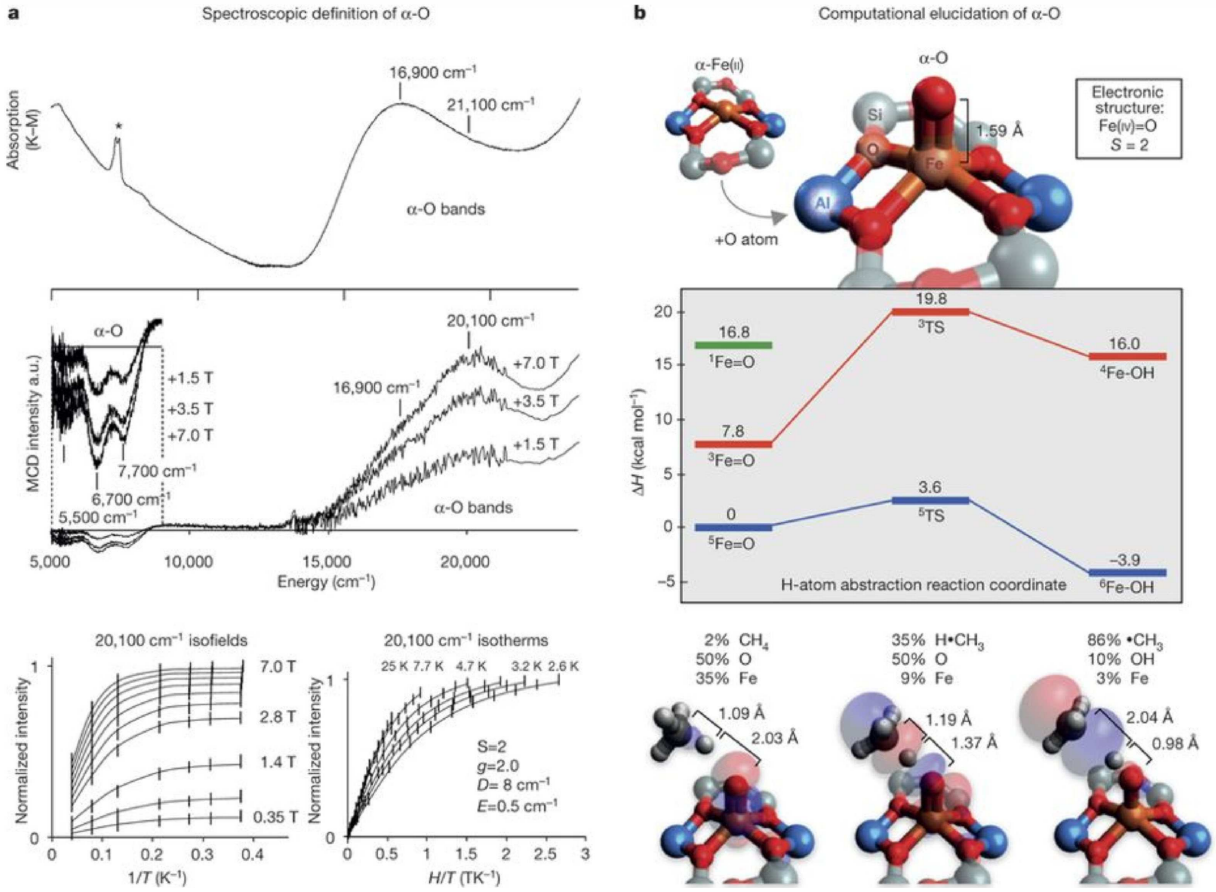

Figure 8. Spectroscopic and computational elucidation of α-O. (a) Top, room-temperature UV-vis data, and middle, 3 K MCD data from N_2O-activated BEA. Bottom, variable-temperature variable-field MCD saturation magnetization data from the 20,100 cm^{-1} band of α-O. (b) Top, DFT-optimized structure of α-Fe (IV) = O in the S = 2 ground state. Middle, energetics of the CH_4 homolytic C–H activation. Bottom, evolution of the lowest unoccupied molecular orbital along the reaction coordinate.[115] Reprinted with permission from *Nature*, 2016, 536, 317. Copyright 2016 Nature publishing group.

attributed to the notable radical character of the oxygen atom at the transition state, corresponding to a highly reactive Fe^{3+}–$O^{\bullet-}$ state (Figure 8). This finding further support the proposal that the radical oxygen is a key factor determining the catalytic activity of the active site for C–H bond activation.[108,116b, 117, 125] Calculations on a broad range of metal-exchanged zeolites by Curet-Arana and co-workers showed that the barrier for C–H bond cleavage is directly related to the energy of the lowest unoccupied molecular orbital (LUMO) and the electronegativity of active site in the metal exchanged zeolites.[126] A periodic hybrid DFT study by Solans-Monfort et al on the interaction of model adsorbents with Cu and Fe-exchanged zeolites highlighted the importance of the local environment of EF sites for their adsorption properties and reactivity.[127]

Nørskov and co-workers have computationally screened the activity of wide variety of oxide- and zeolite-based catalysts for the activation of C–H bonds in methane.[128] It was found that the barrier for the homolytic C–H cleavage in methane linearly correlates with the computed hydrogen affinity of the active site (Figure 9).[128] The computational results pointed to Cu-exchanged zeolites as superior catalysts for methane conversion compared to zeolite-catalysts modified with other cations for a given active site motif. In particular, the scaling relationship is in line with the experimental findings that $[Cu_3(\mu\text{-}O)_3]^{2+}$/MOR has an order of magnitude greater methanol yield (per Cu atom) than other zeolites.[109] Besides, the computational screening identified IrO_2 as a potential new catalyst for methane activation. Further computational analysis revealed that the reactivities of C–H bonds in methane and methanol can be used as the descriptors for predicting selectivity of methane oxidation in a direct continuous process.[129]

However, a recent computational study by Gani and Kulik who considered about 500 model Fe^{2+} compounds for methane oxidation to methanol with N_2O oxidant reveal important limitations of such the predictive models based on the linear scaling relationship approximation.[130] It was shown that the linear relationship for single site catalyst screening holds only when the geometric parameters of iron are fixed. The thermodynamic favorability of both Fe=O and Fe–OH formation and the transition state of Fe=O formation relative to its product can be increased by increasing the out-of-plane distortion of the metal center, which effectively breaks the linear relationship. The computational results also show that the splitting between d_{xz}/d_{yz} and d_{z2} orbitals, other than the

© 2018 The Authors. Published by Wiley-VCH Verlag GmbH & Co. KGaA

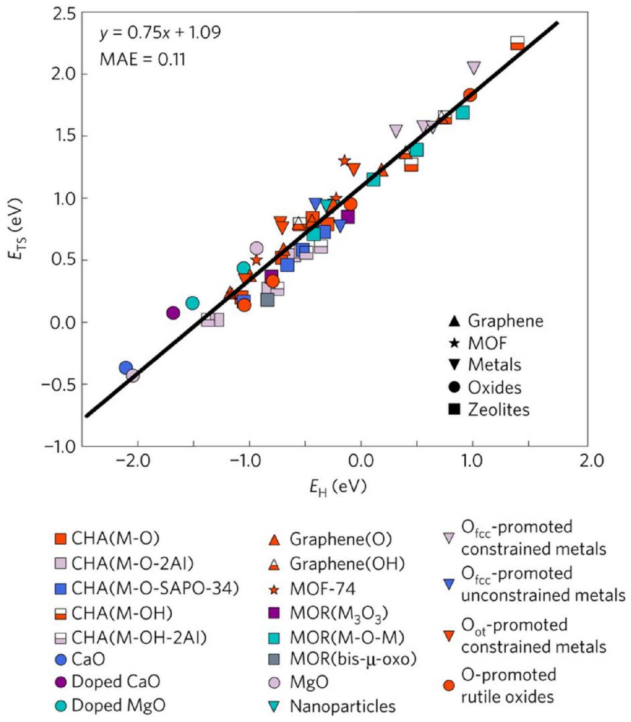

Figure 9. Universal scaling relationship for methane C–H bond activation that proceeds via a radical-like transition state.[128] Reprinted with permission from *Nat. Mater.*, 2016, 16, 225. Copyright 2015 Nature publishing group.

highest occupied molecular orbital (HOMO), is the key factor determining the effectiveness of linear relationship and BEP relationships. Therefore, the authors concluded that one should pay special attention when using such parameters as the HOMO energy level and orbital properties as reactivity descriptors for open-shell single-site catalysts.

Periodic DFT calculations were carried out to study the property-activity relations in dual-metal trinuclear $[Cu_2MO_3]^{2+}$ (M = Fe, Co, Ni) clusters confined in ZSM-5 zeolite.[131] It was found that the activation barrier of the homolytic C–H bond cleavage shows a good linear correlation with the thermochemical stability of the methyl radical intermediate. The hydrogen affinity of the reactive oxygen site is also able to capture the general trend of the catalyst activities (Figure 10a–**b**). The deviations from the clear linear trend were attributed to the fact that although the hydrogen affinity descriptor reflects the intrinsic reactivity of the oxygen site, it does not account for the interactions between the confined methyl radical and zeolite walls. Although the radical nature of the reactive oxygen atom has been proposed earlier to be important for methane oxidation activity,[108,117] calculations did not reveal any correlation between the computed C–H cleavage barrier the atomic spin density of the reactive oxygen site (Figure 10c). These results emphasize the complexity of the property-reactivity relations for methane activation by cationic complexes in confined space. The energetics of methane activation can be influenced by both the intrinsic chemistry of the EF metal-oxo sites and by such secondary effects as the flexibility of the EF species, its local coordination environment and confinement effects due to zeolite pores.

Another intensively studied zeolite-based catalysts is Cu/CHA that exhibits an outstanding performance in the selective catalytic reduction (SCR) of nitrogen oxides.[13a] By integrating aiMD and experimental operando spectroscopy, Paolucci et al reported that, independent of the initial location and the zeolite topology the mononuclear Cu^{2+} and $[CuOH]^+$ cations can quite freely move in the supercages of CHA driven by the solvation effect of NH_3.[132] These NH_3-solvated Cu species are the true active sites promoting the SCR reaction.[110a] Detailed reaction kinetics further released strong evidence that the low-temperature oxidation half-cycle occurs with the participation of a transient $[Cu(NH_3)_2]^+$–O_2–$[Cu(NH_3)_2]^+$ intermediate formed by two isolated Cu species. Instead, at reaction temperatures above 300 °C, NH_3 solvation effect is repealed and as a result, isolated Cu species act as individual active sites.[133] Very recently, Gounder and co-workers further identified that the range of mobility and the possibility of self-aggregation of the NH_3-solvated Cu^{2+} species are determined by the electrostatic potential between the charge-compensating framework Al sites and the cationic $[Cu(NH_3)_2]^{2+}$ complex.[134] The maximum volume of $[Cu(NH_3)_2]^{2+}$ diffusion is the zeolite void with a Cu–Al distance $\leq$ 9 Å (Figure 11). Therefore, it was concluded that the dynamics of the Cu-containing species depends on the concentration of the Cu cations as well as the composition and topology of zeolite framework. A similar reaction-induced dynamics has also been proposed for Mo/ZSM-5 zeolite catalysts active for dehydrogenative aromatization of methane.[98] During methane aromatization, the initially isolated Mo-oxo species are self-organized and carburized into Mo-(oxo)carbide nanoparticle which is a proposed active site for catalytic aromatics production and coke formation. This carburization process is reversible and the initial Mo-oxo species can be regenerated in O_2 atmosphere.

Beyond the Single-Site Approximation: Cooperative and Synergistic Effects

Acid-Base Synergy

The catalytic reactivity of metal-containing zeolites can be contributed by both the chemistry of the EF metal site and the adjacent oxygen atoms that together form Lewis acid-base pairs. The synergistic action of both the acid and the base components of the active site manifests itself in many zeolite-based catalytic systems. Their close proximity gives rise to cooperative effects where both species contribute to the catalytic cycles. The reactivity of the metal site cannot therefore be considered separately from its conjugated base and the active site should rather be regarded as a synergistically cooperating active site ensemble.

Non-oxidative dehydrogenation of light alkanes by Zn- and Ga-containing zeolites is an illustrative example of such acid-base cooperative mechanisms.[135] Experimental and computational studies have been devoted to the investigation of the nature of the active sites and the mechanism of alkane

© 2018 The Authors. Published by Wiley-VCH Verlag GmbH & Co. KGaA

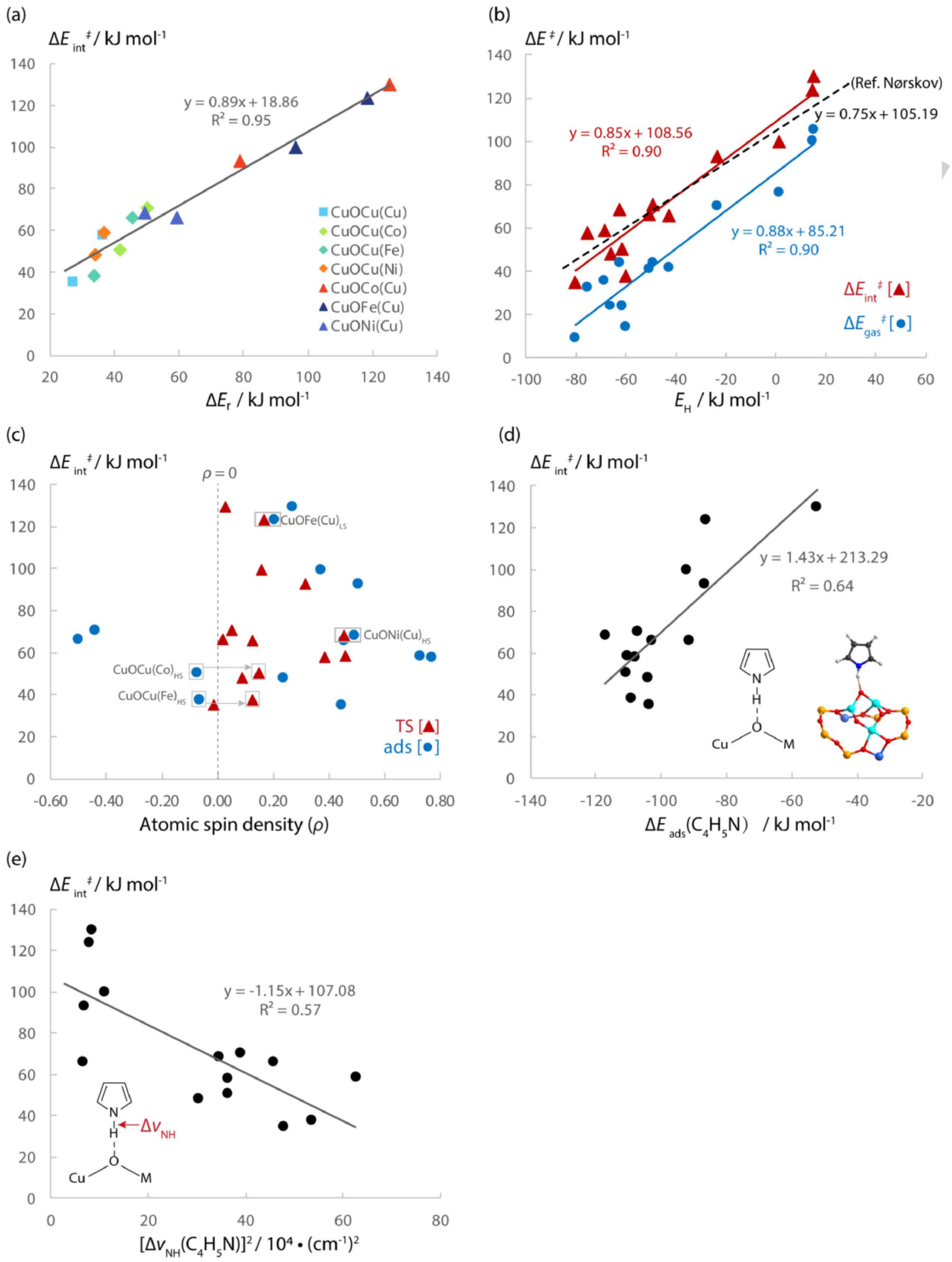

Figure 10. Dependency of methane activation barrier on (a) reaction energy, (b) H affinity, (c) atomic spin density, and basicity probed by (d) pyrrole adsorption energy and (e) N–H vibrational shift.[131] Reprinted with permission from *Small Methods*, 2018, 1800266. Copyright 2018 Wiley.

dehydrogenation by Zn/ZSM-5.[136] A wide range of structural models including isolated Zn^{2+} cations as well as different oxo- and hydroxo-Zn clusters have been proposed as the active sites for alkane activation.[137] All these complexes feature conjugate Lewis acid-base pairs formed by the zinc cation and the adjacent electronegative oxygen centers. They promote the C–H bond activation via a heterolytic mechanism resulting in the formation of a zinc-alkyl fragment and a hydroxyl group.[138] A similar acid-base synergistic mechanism has been proposed for alkane activation by Ga-modified zeolites.[139] The catalytic

© 2018 The Authors. Published by Wiley-VCH Verlag GmbH & Co. KGaA

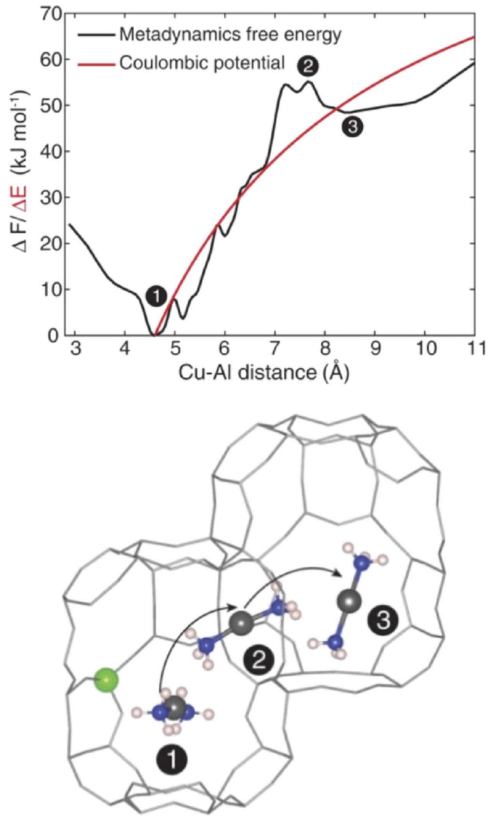

Figure 11. Simulated $[Cu(NH_3)_2]^+$ diffusion up to 11 Å from charge-compensating Al. On left, the metadynamics-computed free energy at 473 K of $[Cu(NH_3)^2]^+$ in CHA supercell versus Cu–Al distance. The red line is the energy profile predicted from a point-charge electrostatic model. Labeled are reactant state (1) ($[Cu(NH_3)_2]^+$ in the same cage as Al), transition state (2) ($[Cu(NH_3)_2]^+$ diffusion through 8-MR), and product state (3) $[Cu(NH_3)_2]^+$ in the neighboring cage without Al). Corresponding $[Cu(NH_3)_2]^+$ configurations from the trajectories are shown on the right.[134] Reprinted with permission from *Science*, 2017, 357, 898. Copyright 2017 Science.

performance of these systems was shown to be defined by both the Lewis acidity of the metal center and the basicity of the adjacent base site.

The acid-base cooperative effects have been shown to be important for the catalytic performance of Fe/ZSM-5.[106g] Periodic DFT calculations revealed that only the isolated Fe^{2+} species could sustain the catalytic cycles, while the oxidation of benzene by other oxygenated species would rather open path towards long-term catalyst deactivation. The associated unwanted paths involve the secondary conversion of the phenol product over the $Fe^{\delta+}$-$O^{\delta-}$ acid-base pairs to form grafted phenolate intermediates that was proposed to act as the precursors for coke formation. This prediction was verified by recent experimental studies employing modern advanced spectroscopic techniques.[115]

Another example is methane oxidation with H_2O_2 over Fe/ZSM-5 zeolite.[140] The activation of the Fe-containing cluster with H_2O_2 gives rise to a variety of Fe^{3+}-oxo and Fe^{4+}-oxo complexes potentially reactive towards methane dissociation.[141] Although homolytic C–H bond dissociation over the basic EF oxygen sites was proposed in the previous work (see discussion and references in earlier sections), the calculation identified additional reaction channels including the heterolytic C–H bond cleavage over an Fe-O acid-base pairs and Fenton-type mechanism involving transient formation of OH radicals. For all reaction pathways, the direct participation and cooperation between the Fe metal site and the adjacent basic oxygen centers were shown to be important.

Similarly, the acid-base synergy was also proposed to be crucial for the efficient conversion of biomass by zeolite catalysts. Bell and co-workers carried out a QM/MM study on the reactivity of lattice-substituted BEA zeolites in glucose to fructose isomerization reaction. Sn-BEA zeolite was predicted to show superior activity and selectivity compared to BEA zeolites modified with other metals such as Ti, Zr, Nb and others.[142] Electronic structure analysis revealed that such a unique catalytic activity should be attributed not only to the polarizability of the Lewis acid sites of the metal atoms, but also to the Brønsted basicity of the oxygen atom in the first coordination shell of the metal center. The negative charge on the oxygen atom can significantly stabilize the reaction intermediates by electrostatic interactions.

Lewis Acid-Brønsted Acid Synergy

Besides the Lewis acid-promoted Brønsted acidity discussed above, the catalytic performance in Lewis acid-catalyzed reactions can also be promoted by secondary interactions with the BASs neighboring cationic site.[16,143-145] The direct cooperation between Lewis acid sites and the neighboring proton donors (Lewis acid-Brønsted acid cooperation) has been shown to play important roles in the catalytic properties of lattice-modified Lewis acid zeolite catalysts such as Sn, Ti and Zr-containing aluminosilicates.[143,145] Large-pore BEA zeolites modified with Lewis acidic Sn sites are active catalysts for selective isomerization of glucose to fructose in water.[146] This reaction is one of the key processes in chemocatalytic conversion schemes for the valorization of cellulosic biomass.[147] There is currently a consensus in the research community that the unique reactivity of Sn-BEA zeolites is related to the presence of open lattice Sn-OH.[18f,88d, 95b, 148] Besides the enhanced flexibility and related higher Lewis acidity of such partially hydrolyzed sites, their catalytic reactivity towards glucose isomerization is also promoted by secondary effects provided by neighboring proton-donating group. Computational studies indicate that the activation barrier of the rate-determining 1,2-H-shift step catalyzed by the Lewis acidic Sn sites can be reduced dramatically when accompanied by the protonation of the aldehyde moiety of hexose by a vicinal silanol moiety or co-adsorbed water molecule (Figure 12).[143] Importantly, multi-site cooperativity appears to be a common feature for other classes of sugar conversion catalysts[149] ranging from homogeneous ionic liquid-mediated chromium (II) salts[150] to enzymatic systems[151] and (doped) oxides.[152]

An alternative conversion path that is glucose epimerization to mannose can also be catalyzed by Sn-beta zeolite but proceeds in the presence of borate salts, which provide a

© 2018 The Authors. Published by Wiley-VCH Verlag GmbH & Co. KGaA

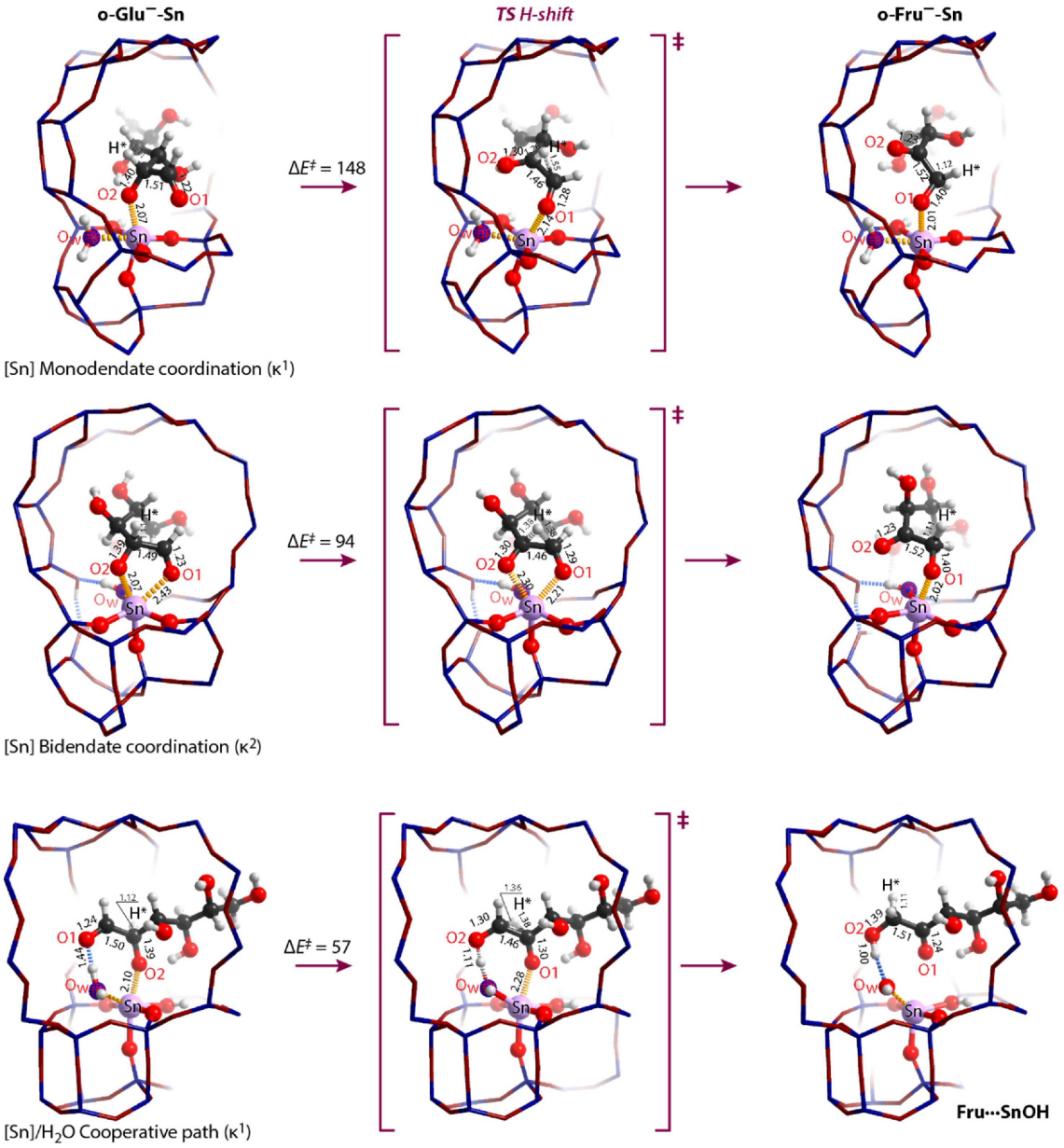

Figure 12. Cooperation between Lewis acidic Sn site and vicinal proton donors play key role in glucose to fructose isomerization. The non-cooperative H-shift paths starting from the monodentate κ1 and bidentate κ2-coordiantion of glucose proceed with substantially higher activation barriers ($\Delta E^{\ddagger}$, kJ mol^{-1}) than the cooperative path, in which the H*-shift between C1 and C2 sites of the hexose is accompanied by the simultaneous protonation of the aldehyde moiety.[143]

somewhat different cooperative strategy. DFT study by Chethana and Mushrif reveals the LAS of Sn and the BAS of silanol groups participate into the 1,2 carbon-shift reaction, and in such a way the barrier of the rate-determining step of enolization is decreased. The borate salt suppresses the competing side-reaction of glucose isomerization by forming complexes with glucose and Sn-OH group, respectively.[153] A similar synergistic effects of Na^+ exchange, proximate silanol motif, and solvents to facilitate the 1,2-carbon shift reaction has been identified in a DFT mechanistic study performed by Yang and Zhou.[154]

The cooperation between Lewis acid and Brønsted acid was also observed for the hydrodeoxygenation of 2,3-butanediol to butane catalyzed by Cu/zeolites.[155] It was found that the hydrogenation and dehydrogenation reactions occur on the Cu sites of the catalysts, while the dehydration reactions takes place on the acid sites of zeolite. DFT simulations suggest that the different location of copper in the zeolites of Cu/ZSM-5 and Cu/Y give rise to distinctly different selectivity in 2,3-butanediol chemistry. The larger cages of Y zeolite enables copper to grow sufficiently large to eventually block the BAS resulting in a higher selectivity to methyl ethyl.

© 2018 The Authors. Published by Wiley-VCH Verlag GmbH & Co. KGaA

Schneider and co-workers combined DFT calculations and site titration to demonstrate that in Cu/SSZ-13 the NO-assisted NH_3 dissociation produces a Cu-bound $ONNH_2$ intermediate and a newly in situ-formed BAS vicinal to Cu^I that binds a catalytically relevant NH_4^+ species during the reduction half-cycle. This NH_4^+ is consumed in the oxidation half-cycle. These experimental and computational findings highlight the bifunctional nature of the Cu/SSZ-13.[157] Very recently, the extraordinary activity of Lewis-Brønsted acid pairs of Ga/H-ZSM-5 for propane dehydrogenation was reported by Schreiber et al.[158] The promotion effect of Lewis-Brønsted acid pairs for methanol to aromatics reaction was also identified for the same system by solid-state NMR spectroscopy.[159] Similar synergetic effect of Lewis-Brønsted acid pair was also found to be crucial for the amination reaction by aluminosilicates. Rimola and co-workers showed computationally the need for a synergistic action of both BAS and LAS on the aluminosilicate surface to establish a favorable reaction path for glycine amination.[160]

Zheng and co-authors recently postulated a new synergetic reaction mechanism for the MTO reaction. They proposed that Brønsted-Lewis acid synergy is necessary for the initial C–C bond formation within the MTO reaction.[156] The proposed mechanism involves the methane-formaldehyde reaction pathway promoted by a cooperation between the proton of the BAS and a LAS of a vicinal EFAl species. A formaldehyde analogue of $[Al–OCH_2]^+$ was identified to be a crucial intermediate for the first C–C bond formation (Scheme 4). This work puts forward an important proposal that the synergy of Brønsted acid and Lewis acid in zeolite catalysts could facilitates the catalytic methanol to olefin reaction, which has been supported by NMR experiments.[161]

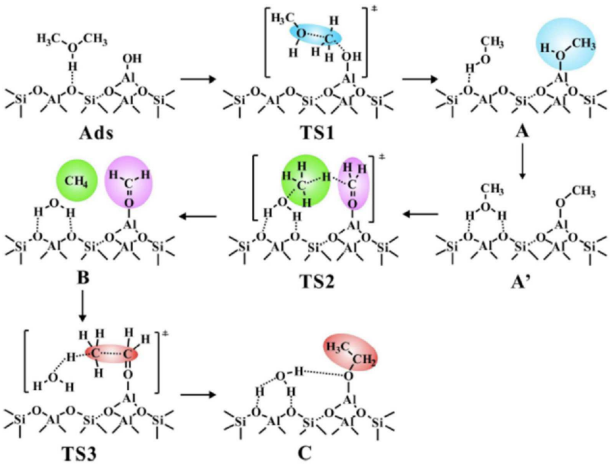

Scheme 4. Proposed mechanism of C–C bond formation at the synergistic Brønsted/Lewis acid sites in zeolite for methanol to olefin reaction.[156] Reprinted with permission from *Chem. Sci.*, 2018, 9, 6470. Copyright 2018 Royal Society of Chemistry.

Confinement-Induced Reactivity and Molecular Recognition Phenomena in Zeolite Catalysis

Cooperative and synergistic effects in multicomponent and multifunctional catalytic systems play important role for the catalytic reactivity. Representative examples can be in biological systems,[162] catalysis by well-defined organometallic complexes,[163] oxide surfaces[152b,164] and supported nanoparticles[165] as well as zeolites.[143b,166] In addition to the synergistic effects arising from the cooperation between the sites of different chemical nature discussed in the previous sections, the presence of multiple sites of the same nature inside the molecular-sized zeolite pores can be crucial for the reactivity and catalytic properties of zeolites. The high density of the active sites in a confined space allows forming multiple interactions with the reactant molecules that define their specific orientation in space, which, in turn, may facilitate and direct their transformations along the predefined paths.[167] This closely resembles the molecular recognition mechanism used by many enzymes and supramolecular catalysts to selectively activate substrates. Such a molecular recognition-type multiple-site reactivity is particularly important for low-silica zeolites featuring high densities of the exchangeable cations in the micropores. To be able to capture such emerging reactivity phenomena, one has to explicitly account for the multifunctional reaction environments when constructing the zeolite models and analyzing the reaction mechanisms.[168] In this section we will discuss recent computational studies highlighting the importance of the multi-site reactivity concepts for the catalytic and adsorption properties of zeolites.

The concept of multi-site reactivity in zeolite catalysis can directly be related to the phenomenon of molecular recognition in enzymatic systems. Molecular recognition is a mechanism enabling selective binding of specific substrates to an active center driven by the formation of multiple secondary interactions with the active site environment.[169] The non-covalent interactions align the reactant in the vicinity of the reactive center in such a way that the transition state of the desirable transformation becomes selectively stabilized[169b,170] Such an induction of chemical reactivity through the formation of multiple interactions appears to be quite common in zeolite chemistry and catalysis.

Alkali-exchanged low-silica zeolites are commonly regarded as the representative examples of base catalysts.[36,171] Their catalytic properties are conventionally attributed to electronegative of lattice oxygens in aluminum-rich frameworks interacting with hard Lewis acidic alkali ions. The hardness of alkali ions and, accordingly, their Lewis acid strength decreases with increasing ionic radius in the order of $Li^+ > Na^+ > K^+ > Rb^+ > Cs^+$. The basicity of the charge-compensating lattice $[AlO_2]^-$ units is a function of the conjugated cation and it increases with increasing cation size.[172] The interactions between the zeolite matrix and the substrate can thus be formed with both the Lewis acidic cations and the basic sites on the zeolite walls. Periodic DFT calculations on faujasite-type zeolite models with realistic chemical composition revealed the

© 2018 The Authors. Published by Wiley-VCH Verlag GmbH & Co. KGaA

crucial role of multi-site interaction for the molecular N_2O_4 adsorption and for the stabilization of the its polar O_2NONO isomer.[173] The adsorption of the latter involves a complex interaction pattern between the cationic NO^+ moiety and the multi-contact stabilization of the NO_3^- fragment by the mobile exchangeable cations. Dispersion interaction were not taken into account in this study as they were assumed to be of relatively minor importance for the molecular species considered.

The dual-site adsorption in alkali-exchanged zeolites has been described for a range of small molecular probes including CO, CO_2, and CH_4.[172c, 174] Dual-site interaction with Lewis acidic extraframework cations and the formation of secondary contacts with the basic framework sites have been demonstrated by a combination of FTIR spectroscopy and quantum chemical calculations.[174a,175] The presence and significance of the secondary interactions with the lattice have been demonstrated for the adsorption of CO_2 on K^+-, Rb^+- or Cs^+-exchanged zeolites Y. Being a weak acid CO_2 can react with the basic lattice sites of FAU framework.[172c,174b] Molecular adsorption of CO_2 involves the formation of both cation-OCO and $O_{framework}$-CO_2 interactions to produce surface carbonates.[172c] Because the strength of CO_2 adsorption follows the expected trend for the zeolite basicity ($Cs^+ > Rb^+ > K^+ > Na^+ > Li^+$), it was proposed that the interaction with the basic framework dominates the CO_2 adsorption by alkali-exchanged FAU zeolites. Nevertheless, the cooperative nature of the interactions with both Lewis acid and Lewis base sites resulting in the formation of surface carbonates should not be neglected.

The importance of the interactions between the guest molecules and both the exchangeable ions and the zeolite lattice has been observed during the adsorption of aromatic compounds in zeolites with FAU topology. At low loading (2-3 molecules per supercage) aromatic compounds adsorb preferentially face-on onto the cationic sites at the SII crystallographic position.[176] The adsorption of aromatic molecules lead to a pronounced contraction of the zeolite unit cells, which was attributed to a dual effect of the decreased cation-framework interaction and the formation of new direct adsorbent-framework interactions.[176a] This hypothesis was validated by the results of FTIR and Raman spectroscopies on xylene adsorption in FAUs that clearly showed the formation of a π-complex between the xylene aromatic system and the alkali cations as well as additional CH···O contacts with the basic lattice.[176b] Whereas toluene and xylenes can only form π-complexes with individual cations or form stacked aggregates at higher loadings, benzene becomes symmetrically aligned in the 12-membered ring window of the supercage as a result of the formation of multiple van der Waals interactions between benzene C–H groups and the framework oxygens.[176c,177] Similarly, the specific alignment of ferrocene in NaY pores has been attributed to the concert effect of multiple weak van der Waals interactions between the cyclopentadienyl ligands and pore walls.[178] These studies emphasize the importance of weak van der Waals interactions on adsorption and molecular recognition properties of zeolites. Despite having small individual contribution, their cumulative power can be strong enough to not only define the preferred adsorption geometry but to even determine the catalytic performances of reactive ensembles inside the zeolite pores.

The difference in van der Waals stabilization of the intermediates defined by the size and shape of zeolite pores was proposed to be the key factor for glucose to fructose isomerization activity of Sn-modified MOR, BEA, MFI and MWW. Despite similar intrinsic reactivity of the Lewis acidic framework Sn sites in these materials, their catalytic performances drastically vary.[179] Periodic calculations showed an increased van der Waals stabilization of the bulky carbohydrate substrates and products in narrow pores of Sn-MFI and Sn-MWW zeolites, which limited their ability to access the catalytic lattice Sn sites.[143b]

The catalytic role of the multi-site interaction with extraframework species has been discussed in a DFT study on the mechanism of N_2O_4 disproportionation over alkali-exchanged FAUs.[166a,173] Periodic DFT calculations revealed that the catalytic performance of the zeolites in these processes does not depend on the individual properties of the reactive sites such as basicity or acidity of the zeolites. It is rather determined by the possibility to form an optimal coordination environment for the anionic product of the disproportionation reaction that is in turn controlled by the size and mobility of the alkali cations inside the FAU structure. A similar hypothesis on the confinement-induced reactivity has also been put forward to explain the photocatalytic activity of alkali-Y zeolites in oxidation of alkenes.[180] Adsorption in low-silica zeolites can involve interaction with more than one exchangeable site. Such a multi-site adsorption mode requires an optimal match between the size of the adsorbent and the zeolite cations at the adjacent sites.

A more recent example of the confinement-induced reactivity in zeolite catalysis is a series of computational works by Rohling et al on Diels-Alder Cycloaddition-dehydration (DACD) reaction between furanic compounds and alkenes by FAU-type zeolites.[181] DACD is considered as an important step in a perspective chemocatalytic technology for the production of aromatic products from renewable cellulosic biomass feedstock.[182] The conversion of dimethylfuran with ethylene over different alkali-exchanged Y zeolites has been studied in detail by periodic DFT calculations complemented with electronic structure analysis, microkinetic modelling and catalytic tests using a range of alkali-exchanged FAU-type zeolites.[181c] The study demonstrated the crucial role of the synergetic effect of the ensemble of cations in the FAU supercage on the DACD reaction. The promoting effect of the zeolite is mainly associated with the confinement effects provided by multiple cations and zeolite framework that give rise to a special alignment of the reactants and the effective stabilization of the transition states (Figure 13).[181a]

The computational analysis of the DACD conversion of substituted furans by alkali-Y zeolites revealed only a minor role of the Lewis acidity of the reactive sites on the catalytic activity, which is to a large extend determined by the geometrical constraints imposed by the size of the cations and the reactants.[181b] It was demonstrated that the presence of electron-donor or acceptor substituents on the furan ring does

© 2018 The Authors. Published by Wiley-VCH Verlag GmbH & Co. KGaA

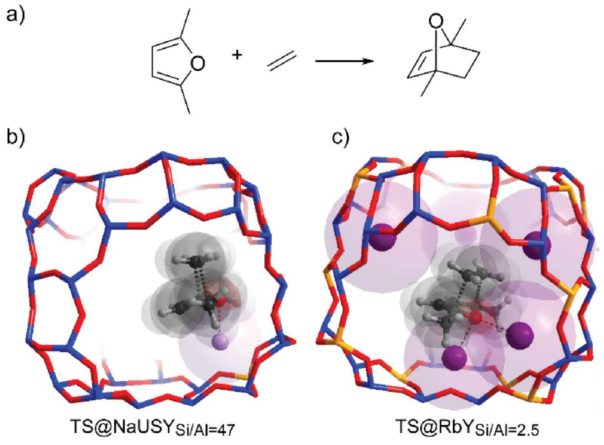

Figure 13. (a) Diels-Alder cycloaddition (DAC) of dimethylfuran and ethylene and (b,c) the respective DFT-optimized transition state for the reaction by a single-site NaUSY (Si/Al = 47) and realistic RbY (Si/Al = 2.5) zeolite models.[168] Reprinted with permission from *ACS Catal.*, 2017, 7, 4230. Copyright 2017 American Chemical Society.

not have a direct effect on the DACD reactivity. The computed barriers are influenced by the steric effects and the strength of the interactions within the zeolite cage. The stabilization of the reactive intermediates is contributed by the multi-site interactions with the extraframework sites and the basic framework.

Concluding Remarks

Computational chemistry plays nowadays crucial role in helping the identification of the nature of the active site and unravelling the reaction mechanism in zeolite catalysis at the atomic level. Theory provides important fundamental insights enabling the detailed assignment of spectroscopic features and helping to identify crucial reaction intermediates. These molecular level insights have been proven crucial for the guided optimization of zeolite catalysts and tailored design of improved catalytic materials. Specifically, DFT calculations have been intensively applied to understand the location and structure of the active site in zeolites and to rationalize the plausible reaction pathways. Experimental catalysis in the past 20 years made a great step forward towards operando spectroscopy and kinetic analysis. Computational chemistry are following the same path by combination of static calculations with microkinetic modelling, ab initio thermodynamics analysis and molecular dynamics simulations. With this, computational chemistry has been gradually bridging the gap between the molecular model and real zeolite catalysts under experimental conditions and providing striking description about the dynamic evolution of the active site and structure-reactivity relationships in zeolite catalysis. Computational modelling also show its advantages to screen and search potential new zeolite catalyst, propose new reaction mechanism or new concept, optimize and design new zeolite catalyst with tailored properties.

However, the zeolite models employed in simulation are often simplified as a "static single-site" including only partial structural representation of the true zeolite catalyst applied in catalytic process. To account for the multiple factors governing the reaction of the complex catalysts, the researchers need to consider such aspects as the formation of bifunctional or multifunctional reactive environment, dynamic compositions and mobility of the reaction centers, real reaction conditions and zeolite confinement effects and so forth. The more complex catalyst models and the alternative reaction channels need to be taken into consideration to address the complexity of the zeolite catalysts. This is recently partially addressed for some of simplified Brønsted acid catalyzed model reactions. However, it is still very challenging for many complex reaction systems. In this context, multiscale computational methods would be helpful to construct a composite methodology that includes all the crucial physical phenomena and to explicitly account for the whole complexity of the underlying catalytic processes.[21]

On the other hand, there are still lack of efficient and robust methodologies which can adequately account for the complex reaction mechanisms. The identification of all elementary steps and reaction intermediates for challenging chemical reactions with large numbers of intermediates is essential for estimating such key reaction parameters as reaction rates, thermodynamics and selectivity. However, building such a framework for detailed analysis is by no means trivial employing well-established electronic-structure methods, even for relatively well-studied reactions where many of the elementary steps are already known. For emerging reactions with little mechanistic precedent, the task requires large amounts of effort, despite that nonequilibrium molecular dynamics and Monto Carlo methods have recently been applied for a few zeolite catalysis systems to help search different reaction routes from a transition state.[49b,72] The development of powerful automated protocols suitable for the exploration of complex reaction networks on the high-dimensional reactive potential energy surfaces more efficiently than the conventional manual expert knowledge-based mechanistic analysis is highly desirable. Increasing efforts have been invested in this direction in recent years.[183] The applications of such methods in zeolite catalysis is anticipated in the near future.

Acknowledgements

E.A.P. acknowledges the partial support from the Government of the Russian Federation (Grant 08-08) and the Ministry of Education and Science of Russian Federation (Project 11.1706.2017/4.6). G.L. thanks NWO for her personal Veni grant (no. 016.Veni.172.034). The authors thank NWO for continuous support of their research by providing access to SurfSARA supercomputer facilities.

Conflict of Interest

The authors declare no conflict of interest.

© 2018 The Authors. Published by Wiley-VCH Verlag GmbH & Co. KGaA

Keywords: Heterogeneous catalysis · Active site cooperativity · Brønsted acid site · Lewis acid site · Computational modelling

[1] C. Martinez, A. Corma, *Coord. Chem. Rev.* **2011**, *255*, 1558–1580.
[2] a) E. T. C. Vogt, B. M. Weckhuysen, *Chem. Soc. Rev.* **2015**, *44*, 7342–7370; b) J. Shi, Y. D. Wang, W. M. Yang, Y. Tang, Z. K. Xie, *Chem. Soc. Rev.* **2015**, *44*, 8877–8903.
[3] U. Olsbye, S. Svelle, M. Bjorgen, P. Beato, T. V. W. Janssens, F. Joensen, S. Bordiga, K. P. Lillerud, *Angew. Chem. Int. Ed.* **2012**, *51*, 5810–5831; *Angew. Chem.* **2012**, *124*, 5910–5933.
[4] a) P. Tomkins, M. Ranocchiari, J. A. van Bokhoven, *Acc. Chem. Res.* **2017**, *50*, 418–425; b) C. Karakaya, R. J. Kee, *Prog. Energy Combust. Sci.* **2016**, *55*, 60–97.
[5] a) H. Li, A. Riisager, S. Saravanamurugan, A. Pandey, R. S. Sangwan, S. Yang, R. Luque, *ACS Catal.* **2018**, *8*, 148–187; b) L. T. Mika, E. Csefalvay, A. Nemeth, *Chem. Rev.* **2018**, *118*, 505–613; c) D. M. Alonso, J. Q. Bond, J. A. Dumesic, *Green Chem.* **2010**, *12*, 1493–1513.
[6] G. Tabacchi, *ChemPhysChem* **2018**, *19*, 1249–1297.
[7] a) Y. V. Kissin, *Catal. Rev.* **2001**, *43*, 85–146; b) J. F. Haw, W. Song, D. M. Marcus, J. B. Nicholas, *Acc. Chem. Res.* **2003**, *36*, 317–326; c) T. F. Degnan, *J. Catal.* **2003**, *216*, 32–46; d) G. Busca, *Chem. Rev.* **2007**, *107*, 5366–5410; e) A. Primo, H. Garcia, *Chem. Soc. Rev.* **2014**, *43*, 7548–7561.
[8] M. Boronat, A. Corma, *Catal. Lett.* **2015**, *145*, 162–172.
[9] a) A. Bhan, E. Iglesia, *Acc. Chem. Res.* **2008**, *41*, 559–567; b) H. Chiang, A. Bhan, *J. Catal.* **2010**, *271*, 251–261; c) E. G. Derouane, J. C. Védrine, R. R. Pinto, P. M. Borges, L. Costa, M. A. N. D. A. Lemos, F. Lemos, F. R. Ribeiro, *Catal. Rev.* **2013**, *55*, 454–515.
[10] a) C. Lee, D. J. Parrillo, R. J. Gorte, W. E. Farneth, *J. Am. Chem. Soc.* **1996**, *118*, 3262–3268; b) R. J. Gorte, *Catal. Lett.* **1999**, *62*, 1–13; c) J. Sauer, *J. Mol. Catal.* **1989**, *54*, 312–323.
[11] N. Kosinov, C. Liu, E. J. M. Hensen, E. A. Pidko, *Chem. Mater.* **2018**, *30*, 3177–3198.
[12] a) B. E. R. Snyder, M. L. Bols, R. A. Schoonheydt, B. F. Sels, E. I. Solomon, *Chem. Rev.* **2018**, *118*, 2718–2768; b) A. R. Kulkarni, Z. J. Zhao, S. Siahrostami, J. K. Norskov, F. Studt, *Catal. Sci. Technol.* **2018**, *8*, 114–123.
[13] a) M. Jablonska, R. Palkovits, *Appl. Catal. B* **2016**, *181*, 332–351; b) J. H. Wang, H. W. Zhao, G. Haller, Y. D. Li, *Appl. Catal. B* **2017**, *202*, 346–354.
[14] a) G. W. Huber, A. Corma, *Angew. Chem. Int. Ed.* **2007**, *46*, 7184–7201; *Angew. Chem.* **2007**, *119*, 7320–7338.
[15] a) M. A. Bañares, *Catal. Today* **1999**, *51*, 319–348; b) Y. Ono, *Catal. Rev.* **1992**, *34*, 179–226; c) A. Bhan, W. N. Delgass, *Catal. Rev.* **2008**, *50*, 19–151.
[16] M. Moliner, *Dalton Trans.* **2014**, *43*, 4197–4208.
[17] a) A. Corma, H. García, *Chem. Rev.* **2002**, *102*, 3837–3892; b) M. Boronat, A. Corma, M. Renz, P. M. Viruela, *Chem. Eur. J.* **2006**, *12*, 7067–7077.
[18] a) Y. Roman-Leshkov, C. J. Barrett, Z. Y. Liu, J. A. Dumesic, *Nature* **2007**, *447*, 982–985; b) H. Y. Luo, J. D. Lewis, Y. Román-Leshkov, *Annu. Rev. Chem. Biomol. Eng.* **2016**, *7*, 663–692; c) A. Corma, L. T. Nemeth, M. Renz, S. Valencia, *Nature* **2001**, *412*, 423–425; d) A. Corma, M. E. Domine, S. Valencia, *J. Catal.* **2003**, *215*, 294–304; e) A. Corma, M. Renz, *Chem. Commun.* **2004**, *5*, 550-551; f) Y. Román-Leshkov, M. Moliner, J. A. Labinger, M. E. Davis, *Angew. Chem. Int. Ed.* **2010**, *49*, 8954–8957; *Angew. Chem.* **2010**, *122*, 9138–9141; g) R. Bermejo-Deval, R. S. Assary, E. Nikolla, M. Moliner, Y. Román-Leshkov, S.-J. Hwang, A. Palsdottir, D. Silverman, R. F. Lobo, L. A. Curtiss, M. E. Davis, *Proc. Natl. Acad. Sci. India* **2012**, *109*, 9727–9732; h) W. R. Gunther, Y. Wang, Y. Ji, V. K. Michaelis, S. T. Hunt, R. G. Griffin, Y. Roman-Leshkov, *Nat. Commun.* **2012**, *3*, 1109.
[19] a) V. Van Speybroeck, K. Hemelsoet, L. Joos, M. Waroquier, R. G. Bell, C. R. A. Catlow, *Chem. Soc. Rev.* **2015**, *44*, 7044–7111; b) V. Van Speybroeck, K. De Wispelaere, J. Van der Mynsbrugge, M. Vandichel, K. Hemelsoet, M. Waroquier, *Chem. Soc. Rev.* **2014**, *43*, 7326–7357.
[20] a) S. Svelle, C. Tuma, X. Rozanska, T. Kerber, J. Sauer, *J. Am. Chem. Soc.* **2009**, *131*, 816–825; b) G. Piccini, M. Alessio, J. Sauer, *Angew. Chem. Int. Ed.* **2016**, *55*, 5235–5237; *Angew. Chem.* **2016**, *128*, 5321–5323; c) N. Mardirossian, M. Head-Gordon, *Mol. Phys.* **2017**, *115*, 2315–2372; d) R. Peverati, D. G. Truhlar, *Phil Trans. R. Soc. A* **2014**, *372*, 20120476.
[21] C. J. Heard, L. S. Grajciar, A. A. Bondarenko, M. V. Polynski, J. Meeprasert, E. A. Pidko, P. Nachtigall, *Chem. Soc. Rev.* **2018**, *47*, 8307–8348 .
[22] a) G. Li, E. A. Pidko, R. A. van Santen, C. Li, E. J. M. Hensen, *J. Phys. Chem. C* **2013**, *117*, 413–426; b) C. Liu, G. Li, E. J. M. Hensen, E. A. Pidko, *ACS Catal.* **2015**, *5*, 7024–7033.
[23] A. Laio, M. Parrinello, *Proc. Natl. Acad. Sci. U.S.A.* **2002**, *99*, 12562–12566.
[24] a) J. Kastner, *WIREs Comput. Mol. Sci.* **2011**, *1*, 932–942; b) G. M. Torrie, J. P. Valleau, *J. Comp. Physiol.* **1977**, *23*, 187–199.
[25] a) M. Sprik, G. Ciccotti, *J. Chem. Phys.* **1998**, *109*, 7737–7744; b) E. Darve, D. Rodríguez-Gómez, A. Pohorille, *J. Chem. Phys.* **2008**, *128*, 144120.
[26] J. G. López, G. Vayner, U. Lourderaj, S. V. Addepalli, S. Kato, W. A. deJong, T. L. Windus, W. L. Hase, *J. Am. Chem. Soc.* **2007**, *129*, 9976–9985.
[27] a) S. Wang, P. Wang, Z. Qin, Y. Chen, M. Dong, J. Li, K. Zhang, P. Liu, J. Wang, W. Fan, *ACS Catal.* **2018**, *8*, 5485–5505; b) K. Chen, M. Abdolrhamani, E. Sheets, J. Freeman, G. Ward, J. L. White, *J. Am. Chem. Soc.* **2017**, *139*, 18698–18704.
[28] a) S. Stepan, D. Jiří, L. Chengbin, W. Blanka, G. Vendula, S. Marek, S. Joachim, *Angew. Chem. Int. Ed.* **2007**, *46*, 7286–7289; *Angew. Chem.* **2007**, *119*, 7424–7427; b) S. Sklenak, J. Dedecek, C. Li, B. Wichterlova, V. Gabova, M. Sierka, J. Sauer, *Phys. Chem. Chem. Phys.* **2009**, *11*, 1237–1247; c) J. Dědeček, S. Sklenak, C. Li, F. Gao, J. Brus, Q. Zhu, T. Tatsumi, *J. Phys. Chem. C* **2009**, *113*, 14454–14466; d) Z. Yu, A. Zheng, Q. Wang, L. Chen, J. Xu, J. Amoureux, F. Deng, *Angew. Chem. Int. Ed.* **2010**, *49*, 8657–8661; *Angew. Chem.* **2010**, *122*, 8839–8843; e) J. Dedecek, M. J. Lucero, C. Li, F. Gao, P. Klein, M. Urbanova, Z. Tvaruzkova, P. Sazama, S. Sklenak, *J. Phys. Chem. C* **2011**, *115*, 11056–11064.
[29] J. A. van Bokhoven, T.-L. Lee, M. Drakopoulos, C. Lamberti, S. Thieß, J. Zegenhagen, *Nat. Mater.* **2008**, *7*, 551.
[30] A. Vjunov, J. L. Fulton, T. Huthwelker, S. Pin, D. Mei, G. K. Schenter, N. Govind, D. M. Camaioni, J. Z. Hu, J. A. Lercher, *J. Am. Chem. Soc.* **2014**, *136*, 8296–8306.
[31] T. Demuth, J. Hafner, L. Benco, H. Toulhoat, *J. Phys. Chem. B* **2000**, *104*, 4593–4607.
[32] L. Benco, T. Demuth, J. Hafner, *J. Chem. Phys.* **1999**, *111*, 7537–7545.
[33] A. J. Jones, E. Iglesia, *ACS Catal.* **2015**, *5*, 5741–5755.
[34] A. Janda, A. T. Bell, *J. Am. Chem. Soc.* **2013**, *135*, 19193–19207.
[35] a) C. Song, Y. Chu, M. Wang, H. Shi, L. Zhao, X. Guo, W. Yang, J. Shen, N. Xue, L. Peng, W. Ding, *J. Catal.* **2017**, *349*, 163–174; b) C. T. Yang, A. Janda, A. T. Bell, L. C. Lin, *J. Phys. Chem. C* **2018**, *122*, 9397–9410.
[36] R. A. Schoonheydt, P. Geerlings, E. A. Pidko, R. A. van Santen, *J. Mater. Chem.* **2012**, *22*, 18705–18717.
[37] P. Sarv, T. Tuherm, E. Lippmaa, K. Keskinen, A. Root, *J. Phys. Chem.* **1995**, *99*, 13763–13768.
[38] Y. Wang, D. Zhou, G. Yang, X. Liu, D. Ma, D. Liang, X. Bao, *Chem. Phys. Lett.* **2004**, *388*, 363–366.
[39] A. Rimola, C. M. Zicovich-Wilson, R. Dovesi, P. Ugliengo, *J. Chem. Theory Comput.* **2010**, *6*, 1341–1350.
[40] T. Baba, Y. Ono, *Appl. Catal. A* **1999**, *181*, 227–238.
[41] J. T. Fermann, S. Auerbach, *J. Chem. Phys.* **2000**, *112*, 6787–6794.
[42] R. Osuga, T. Yokoi, K. Doitomi, H. Hirao, J. N. Kondo, *J. Phys. Chem. C* **2017**, *121*, 25411–25420.
[43] M. E. Franke, U. Simon, *ChemPhysChem* **2004**, *5*, 465–472.
[44] V. Termath, F. Haase, J. Sauer, J. Hutter, M. Parrinello, *J. Am. Chem. Soc.* **1998**, *120*, 8512–8516.
[45] L. Smith, A. K. Cheetham, R. E. Morris, L. Marchese, J. M. Thomas, P. A. Wright, J. Chen, *Science* **1996**, *271*, 799–802.
[46] A. Vjunov, M. Wang, N. Govind, T. Huthwelker, H. Shi, D. Mei, J. L. Fulton, J. A. Lercher, *Chem. Mater.* **2017**, *29*, 9030–9042.
[47] A. Zheng, B. Han, B. Li, S.-B. Liu, F. Deng, *Chem. Commun.* **2012**, *48*, 6936–6938.
[48] a) E. Nusterer, P. E. Blöchl, K. Schwarz, *Chem. Phys. Lett.* **1996**, *253*, 448–455; b) S. Jungsuttiwong, J. Limtrakul, T. N. Truong, *J. Phys. Chem. B* **2005**, *109*, 13342–13351; c) H. Li, S. D. Mahanti, T. J. Pinnavaia, *J. Phys. Chem. B* **2005**, *109*, 21908–21914; d) M. V. Vener, X. Rozanska, J. Sauer, *Phys. Chem. Chem. Phys.* **2009**, *11*, 1702–1712; e) M. Fischer, *Phys. Chem. Chem. Phys.* **2016**, *18*, 15738–15750.
[49] a) S. L. C. Moors, K. De Wispelaere, J. Van der Mynsbrugge, M. Waroquier, V. Van Speybroeck, *ACS Catal.* **2013**, *3*, 2556–2567; b) K. De Wispelaere, B. Ensing, A. Ghysels, E. J. Meijer, V. Van Speybroeck, *Chem. Eur. J.* **2015**, *21*, 9385–9396; c) K. De Wispelaere, C. S. Wondergem, B. Ensing, K. Hemelsoet, E. J. Meijer, B. M. Weckhuysen, V. Van Speybroeck, J. Ruiz-Martínez, *ACS Catal.* **2016**, *6*, 1991–2002.
[50] W. Zhang, Y. Chu, Y. Wei, X. Yi, S. Xu, J. Huang, M. Zhang, A. Zheng, F. Deng, Z. Liu, *Microporous Mesoporous Mater.* **2016**, *231*, 216–229.
[51] S. Li, Y. Zheng, F. Gao, J. Szanyi, W. F. Schneider, *ACS Catal.* **2017**, *7*, 5087–5096.

© 2018 The Authors. Published by Wiley-VCH Verlag GmbH & Co. KGaA

[52] X. Solans-Monfort, M. Sodupe, V. Branchadell, J. Sauer, R. Orlando, P. Ugliengo, *J. Phys. Chem. B* **2005**, *109*, 3539–3545.
[53] a) R. Beaumont, Barthome. D, *J. Catal.* **1972**, *26*, 218–225; b) R. J. Mikovsky, J. F. Marshall, *J. Catal.* **1976**, *44*, 170–173; c) D. Barthomeuf, *J. Phys. Chem.* **1979**, *83*, 249–256; d) A. Zecchina, F. Geobaldo, G. Spoto, S. Bordiga, G. Ricchiardi, R. Buzzoni, G. Petrini, *J. Phys. Chem.* **1996**, *100*, 16584–16599; e) A. Zecchina, R. Buzzoni, S. Bordiga, F. Geobaldo, D. Scarano, G. Ricchiardi, G. Spoto, in *Stud. Surf. Sci. Catal., Vol. 97* (Eds.: L. Bonneviot, S. Kaliaguine), Elsevier, **1995**, pp. 213–222; f) R. A. van Santen, G. J. Kramer, *Chem. Rev.* **1995**, *95*, 637–660.
[54] a) K. Chakarova, K. Hadjiivanov, *J. Phys. Chem. C* **2011**, *115*, 4806–4817; b) C. O. Arean, M. R. Delgado, P. Nachtigall, H. V. Thang, M. Rubes, R. Bulanek, P. Chlubna-Eliasova, *Phys. Chem. Chem. Phys.* **2014**, *16*, 10129–10141; c) J. A. Lercher, C. Gründling, G. Eder-Mirth, *Catal. Today* **1996**, *27*, 353–376.
[55] C. Liu, G. Li, E. J. M. Hensen, E. A. Pidko, *J. Catal.* **2016**, *344*, 570–577.
[56] a) A. J. Jones, R. T. Carr, S. I. Zones, E. Iglesia, *J. Catal.* **2014**, *312*, 58–68; b) J. Macht, R. T. Carr, E. Iglesia, *J. Catal.* **2009**, *264*, 54–66; c) J. Macht, R. T. Carr, E. Iglesia, *J. Am. Chem. Soc.* **2009**, *131*, 6554–6565.
[57] M. Niwa, K. Suzuki, N. Morishita, G. Sastre, K. Okumura, N. Katada, *Catal. Sci. Technol.* **2013**, *3*, 1919–1927.
[58] a) C.-M. Wang, R. Y. Brogaard, B. M. Weckhuysen, J. K. Nørskov, F. Studt, *J. Phys. Chem. Lett.* **2014**, *5*, 1516–1521; b) P. Deshlahra, E. Iglesia, *ACS Catal.* **2016**, *6*, 5386–5392.
[59] a) P. Borges, R. Ramos Pinto, M. A. N. D. A. Lemos, F. Lemos, J. C. Védrine, E. G. Derouane, F. Ramôa Ribeiro, *J. Mol. Catal. A* **2005**, *229*, 127–135; b) N. Katada, S. Sota, N. Morishita, K. Okumura, M. Niwa, *Catal. Sci. Technol.* **2015**, *5*, 1864–1869.
[60] R. Y. Brogaard, C.-M. Wang, F. Studt, *ACS Catal.* **2014**, *4*, 4504–4509.
[61] C. Liu, I. Tranca, R. A. van Santen, E. J. M. Hensen, E. A. Pidko, *J. Phys. Chem. C* **2017**, *121*, 23520–23530.
[62] a) R. Gounder, E. Iglesia, *J. Am. Chem. Soc.* **2009**, *131*, 1958–1971; b) R. Gounder, E. Iglesia, *Acc. Chem. Res.* **2012**, *45*, 229–238.
[63] T. Liang, J. Chen, Z. Qin, J. Li, P. Wang, S. Wang, G. Wang, M. Dong, W. Fan, J. Wang, *ACS Catal.* **2016**, *6*, 7311–7325.
[64] X. Li, J. Jiang, *Phys. Chem. Chem. Phys.* **2018**, *20*, 14322–14330.
[65] D. H. Mei, J. A. Lercher, *AIChE J.* **2017**, *63*, 172–184.
[66] H. Shi, S. Eckstein, A. Vjunov, D. M. Camaioni, J. A. Lercher, *Nat. Commun.* **2017**, *8*, 15442.
[67] a) T. Bucko, L. Benco, J. Hafner, J. G. Angyan, *J. Catal.* **2007**, *250*, 171–183; b) T. Bucko, L. Benco, O. Dubay, C. Dellago, J. Hafner, *J. Chem. Phys.* **2009**, *131*.
[68] T. Bucko, J. Hafner, *J. Phys. Condens. Matter* **2010**, *22*, 384201.
[69] T. Bučko, L. Benco, J. Hafner, J. G. Ángyán, *J. Catal.* **2011**, *279*, 220–228.
[70] D. Tranca, N. Hansen, J. A. Swisher, B. Smit, F. Keil, *J. Phys. Chem. C* **2012**, *116*, 23408–23417.
[71] P. Martin Zimmerman, D. Tranca, J. Gomes, D. Lambrecht, M. Head-Gordon, A. Bell, *J. Am. Chem. Soc.* **2012**, *134*, 19468–19476.
[72] D. C. Tranca, P. M. Zimmerman, J. Gomes, D. Lambrecht, F. J. Keil, M. Head-Gordon, A. T. Bell, *J. Phys. Chem. C* **2015**, *119*, 28836–28853.
[73] a) S. Mallikarjun Sharada, P. M. Zimmerman, A. T. Bell, M. Head-Gordon, *J. Phys. Chem. C* **2013**, *117*, 12600–12611; b) A. Janda, B. Vlaisavljevich, L.-C. Lin, B. Smit, A. T. Bell, *J. Am. Chem. Soc.* **2016**, *138*, 4739–4756; c) J. Van der Mynsbrugge, A. Janda, S. Mallikarjun Sharada, L.-C. Lin, V. Van Speybroeck, M. Head-Gordon, A. T. Bell, *ACS Catal.* **2017**, *7*, 2685–2697; d) A. Janda, B. Vlaisavljevich, B. Smit, L.-C. Lin, A. T. Bell, *J. Phys. Chem. C* **2017**, *121*, 1618–1638.
[74] a) S. M. Babitz, B. A. Williams, J. T. Miller, R. Q. Snurr, W. O. Haag, H. H. Kung, *Appl. Catal. A* **1999**, *179*, 71–86; b) J. A. van Bokhoven, B. A. Williams, W. Ji, D. C. Koningsberger, H. H. Kung, J. T. Miller, *J. Catal.* **2004**, *224*, 50–59; c) B. Xu, C. Sievers, S. B. Hong, R. Prins, J. A. van Bokhoven, *J. Catal.* **2006**, *244*, 163–168; d) J. A. van Bokhoven, B. Xu, in *Stud. Surf. Sci. Catal., Vol. 170* (Eds.: R. Xu, Z. Gao, J. Chen, W. Yan), Elsevier, **2007**, pp. 1167–1173.
[75] C. E. Ramachandran, B. A. Williams, J. A. van Bokhoven, J. T. Miller, *J. Catal.* **2005**, *233*, 100–108.
[76] a) S. Li, A. Zheng, Y. Su, H. Fang, W. Shen, Z. Yu, L. Chen, F. Deng, *Phys. Chem. Chem. Phys.* **2010**, *12*, 3895–3903; b) M. Sami, S. Stian, B. F. Lønstad, S. Ole, *Angew. Chem. Int. Ed.* **2012**, *51*, 652–655; *Angew. Chem.* **2012**, *124*, 676–679.
[77] a) S. J. DeCanio, J. R. Sohn, P. O. Fritz, J. H. Lunsford, *J. Catal.* **1986**, *101*, 132–141; b) J. R. Sohn, S. J. DeCanio, P. O. Fritz, J. H. Lunsford, *J. Phys. Chem.* **1986**, *90*, 4847–4851; c) R. A. Beyerlein, G. B. McVicker, L. N. Yacullo, J. J. Ziemiak, *J. Phys. Chem.* **1988**, *92*, 1967–1970.
[78] a) S. M. T. Almutairi, B. Mezari, G. A. Filonenko, P. C. M. M. Magusin, M. S. Rigutto, E. A. Pidko, E. J. M. Hensen, *ChemCatChem* **2013**, *5*, 452–466; b) S. Li, A. Zheng, Y. Su, H. Zhang, L. Chen, J. Yang, C. Ye, F. Deng, *J. Am. Chem. Soc.* **2007**, *129*, 11161–11171.
[79] a) B. Xu, S. Bordiga, R. Prins, J. A. van Bokhoven, *Appl. Catal. A* **2007**, *333*, 245–253; b) R. Gounder, A. J. Jones, R. T. Carr, E. Iglesia, *J. Catal.* **2012**, *286*, 214–223; c) S. Schallmoser, T. Ikuno, M. F. Wagenhofer, R. Kolvenbach, G. L. Haller, M. Sanchez-Sanchez, J. A. Lercher, *J. Catal.* **2014**, *316*, 93–102.
[80] X. Yi, K. Liu, W. Chen, J. Li, S. Xu, C. Li, Y. Xiao, H. Liu, X. Guo, S.-B. Liu, A. Zheng, *J. Am. Chem. Soc.* **2018**, *140*, 10764–10774.
[81] a) D. L. Bhering, A. Ramírez-Solís, C. J. A. Mota, *J. Phys. Chem. B* **2003**, *107*, 4342–4347; b) C. J. A. Mota, D. L. Bhering, N. Rosenbach, *Angew. Chem. Int. Ed.* **2004**, *43*, 3050–3053; *Angew. Chem.* **2004**, *116*, 3112–3115.
[82] a) A. V. Larin, G. M. Zhidomirov, *J. Struct. Chem.* **2014**, *55*, 583–594; b) J. Jiao, J. Kanellopoulos, W. Wang, S. S. Ray, H. Foerster, D. Freude, M. Hunger, *Phys. Chem. Chem. Phys.* **2005**, *7*, 3221–3226; c) J. Huang, Y. Jiang, V. R. R. Marthala, B. Thomas, E. Romanova, M. Hunger, *J. Phys. Chem. C* **2008**, *112*, 3811–3818.
[83] G. Agostini, C. Lamberti, L. Palin, M. Milanesio, N. Danilina, B. Xu, M. Janousch, J. A. van Bokhoven, *J. Am. Chem. Soc.* **2010**, *132*, 667–678.
[84] a) F. Schüßler, E. A. Pidko, R. Kolvenbach, C. Sievers, E. J. M. Hensen, R. A. van Santen, J. A. Lercher, *J. Phys. Chem. C* **2011**, *115*, 21763–21776; b) C. Liu, R. A. van Santen, A. Poursaeidesfahani, T. J. H. Vlugt, E. A. Pidko, E. J. M. Hensen, *ACS Catal.* **2017**, *7*, 8613–8627.
[85] G. Li, C. Liu, R. Rohling, E. J. M. Hensen, E. A. Pidko, in *Modelling and Simulation in the Science of Micro- and Meso-Porous Materials* (Eds.: C. R. A. Catlow, V. Van Speybroeck, R. A. van Santen), Elsevier, **2018**, pp. 229–263.
[86] P. Y. Dapsens, C. Mondelli, J. Perez-Ramirez, *Chem. Soc. Rev.* **2015**, *44*, 7025–7043.
[87] D. Kubicka, I. Kubickova, J. Cejka, *Catal. Rev.* **2013**, *55*, 1–78.
[88] a) P. Wolf, M. Valla, A. J. Rossini, A. Comas-Vives, F. Núñez-Zarur, B. Malaman, A. Lesage, L. Emsley, C. Copéret, I. Hermans, *Angew. Chem. Int. Ed.* **2014**, *53*, 10179–10183; *Angew. Chem.* **2014**, *126*, 10343–10347; b) J. Dijkmans, J. Demol, K. Houthoofd, S. G. Huang, Y. Pontikes, B. Sels, *J. Catal.* **2015**, *330*, 545–557; c) J. Dijkmans, M. Dusselier, W. Janssens, M. Trekels, A. Vantomme, E. Breynaert, C. Kirschhock, B. F. Sels, *ACS Catal.* **2016**, *6*, 31–46; d) J. W. Harris, M. J. Cordon, J. R. Di Iorio, J. C. Vega-Vila, F. H. Ribeiro, R. Gounder, *J. Catal.* **2016**, *335*, 141–154; e) P. Wolf, M. Valla, F. Núñez-Zarur, A. Comas-Vives, A. J. Rossini, C. Firth, H. Kallas, A. Lesage, L. Emsley, C. Copéret, I. Hermans, *ACS Catal.* **2016**, *6*, 4047–4063.
[89] P. Wolf, W. Liao, T. Ong, M. Valla, J. W. Harris, R. Gounder, W. N. P. Graaff, E. A. Pidko, E. J. M. Hensen, P. Ferrini, J. Dijkmans, B. F. Sels, I. Hermans, C. Copéret, *Helv. Chim. Acta* **2016**, *99*, 916–927.
[90] S. Bordiga, E. Groppo, G. Agostini, J. A. van Bokhoven, C. Lamberti, *Chem. Rev.* **2013**, *113*, 1736–1850.
[91] R. C. Deka, V. A. Nasluzov, E. A. Ivanova Shor, A. M. Shor, G. N. Vayssilov, N. Rösch, *J. Phys. Chem. B* **2005**, *109*, 24304–24310.
[92] S. Shetty, B. S. Kulkarni, D. G. Kanhere, A. Goursot, S. Pal, *J. Phys. Chem. B* **2008**, *112*, 2573–2579.
[93] G. Yang, E. A. Pidko, E. J. M. Hensen, *J. Phys. Chem. C* **2013**, *117*, 3976–3986.
[94] M. Boronat, P. Concepción, A. Corma, M. Renz, S. Valencia, *J. Catal.* **2005**, *234*, 111–118.
[95] a) D. H. Wells, W. N. Delgass, K. T. Thomson, *J. Am. Chem. Soc.* **2004**, *126*, 2956–2962; b) R. Bermejo-Deval, M. Orazov, R. Gounder, S.-J. Hwang, M. E. Davis, *ACS Catal.* **2014**, *4*, 2288–2297.
[96] T. R. Josephson, G. R. Jenness, D. G. Vlachos, S. Caratzoulas, *Microporous Mesoporous Mater.* **2017**, *245*, 45–50.
[97] P. Ferrini, J. Dijkmans, R. De Clercq, S. Van de Vyver, M. Dusselier, P. A. Jacobs, B. F. Sels, *Coord. Chem. Rev.* **2017**, *343*, 220–255.
[98] J. Gao, Y. T. Zheng, J. M. Jehng, Y. D. Tang, I. E. Wachs, S. G. Podkolzin, *Science* **2015**, *348*, 686–690.
[99] a) A. Hagen, F. Roessner, *Catal. Rev.* **2000**, *42*, 403–437; b) Y. T. Cheng, J. Jae, J. Shi, W. Fan, G. W. Huber, *Angew. Chem. Int. Ed.* **2012**, *51*, 1387–1390; *Angew. Chem.* **2012**, *124*, 1416–1419.
[100] a) E. J. M. Hensen, E. A. Pidko, N. Rane, R. A. van Santen, *Angew. Chem. Int. Ed.* **2007**, *46*, 7273–7276; *Angew. Chem.* **2007**, *119*, 7411–7414; b) N. Rane, A. R. Overweg, V. B. Kazansky, R. A. van Santen, E. J. M. Hensen, *J. Catal.* **2006**, *239*, 478–485.
[101] E. A. Pidko, E. J. M. Hensen, R. A. van Santen, *J. Phys. Chem. C* **2007**, *111*, 13068–13075.

© 2018 The Authors. Published by Wiley-VCH Verlag GmbH & Co. KGaA

[102] a) E. A. Pidko, E. J. M. Hensen, G. M. Zhidomirov, R. A. van Santen, *J. Catal.* **2008**, *255*, 139–143; b) E. A. Pidko, R. A. van Santen, E. J. M. Hensen, *Phys. Chem. Chem. Phys.* **2009**, *11*, 2893–2902.
[103] E. A. Pidko, E. J. M. Hensen, R. A. van Santen, *Proc. R. Soc. A* **2012**, *468*, 2070–2086.
[104] a) R. Joyner, M. Stockenhuber, *J. Phys. Chem. B* **1999**, *103*, 5963–5976; b) L. J. Lobree, I.-C. Hwang, J. A. Reimer, A. T. Bell, *J. Catal.* **1999**, *186*, 242–253; c) A. V. Kucherov, M. Shelef, *J. Catal.* **2000**, *195*, 106–112.
[105] a) G. I. Panov, A. K. Uriarte, M. A. Rodkin, V. I. Sobolev, *Catal. Today* **1998**, *41*, 365–385; b) E. T. C. Vogt, G. T. Whiting, A. Dutta Chowdhury, B. M. Weckhuysen, *Adv. Catal.* **2015**, *58*, 143–314; c) R. Zhang, N. Liu, Z. Lei, B. Chen, *Chem. Rev.* **2016**, *116*, 3658–3721.
[106] a) E. J. M. Hensen, Q. Zhu, M. M. R. M. Hendrix, A. R. Overweg, P. J. Kooyman, M. V. Sychev, R. A. van Santen, *J. Catal.* **2004**, *221*, 560–574; b) Q. Zhu, R. M. van Teeffelen, R. A. van Santen, E. J. M. Hensen, *J. Catal.* **2004**, *221*, 575–583; c) K. Yoshizawa, Y. Shiota, T. Yumura, T. Yamabe, *J. Phys. Chem. B* **2000**, *104*, 734–740; d) A. L. Yakovlev, G. M. Zhidomirov, R. A. van Santen, *J. Phys. Chem. B* **2001**, *105*, 12297–12302; e) M. F. Fellah, R. A. van Santen, I. Onal, *J. Phys. Chem. C* **2009**, *113*, 15307–15313; f) M. F. Fellah, I. Onal, R. A. van Santen, *J. Phys. Chem. C* **2010**, *114*, 12580–12589; g) G. Li, E. A. Pidko, R. A. van Santen, Z. Feng, C. Li, E. J. M. Hensen, *J. Catal.* **2011**, *284*, 194–206.
[107] a) K. Reuter, M. Scheffler, *Phys. Rev. Lett.* **2003**, *90*, 046103; b) K. Reuter, in *Operando Research in Heterogeneous Catalysis* (Eds.: J. Frenken, I. Groot), Springer International Publishing, Cham, **2017**, pp. 151–188.
[108] G. Li, P. Vassilev, M. Sanchez-Sanchez, J. A. Lercher, E. J. M. Hensen, E. A. Pidko, *J. Catal.* **2016**, *338*, 305–312.
[109] S. Grundner, M. A. C. Markovits, G. Li, M. Tromp, E. A. Pidko, E. J. M. Hensen, A. Jentys, M. Sanchez-Sanchez, J. A. Lercher, *Nat. Commun.* **2015**, *6*, 7546.
[110] a) C. Paolucci, A. A. Parekh, I. Khurana, J. R. Di Iorio, H. Li, J. D. Albarracin Caballero, A. J. Shih, T. Anggara, W. N. Delgass, J. T. Miller, F. H. Ribeiro, R. Gounder, W. F. Schneider, *J. Am. Chem. Soc.* **2016**, *138*, 6028–6048; b) L. Chen, H. Falsig, T. V. W. Janssens, H. Grönbeck, *J. Catal.* **2018**, *358*, 179–186; c) J. S. McEwen, T. Anggara, W. F. Schneider, V. F. Kispersky, J. T. Miller, W. N. Delgass, F. H. Ribeiro, *Catal. Today* **2012**, *184*, 129–144.
[111] H. A. Doan, Z. Li, O. K. Farha, J. T. Hupp, R. Q. Snurr, *Catal. Today* **2018**, *312*, 2–9.
[112] a) M. H. Groothaert, P. J. Smeets, B. F. Sels, P. A. Jacobs, R. A. Schoonheydt, *J. Am. Chem. Soc.* **2005**, *127*, 1394–1395; b) M. J. Wulfers, S. Teketel, B. Ipek, R. F. Lobo, *Chem. Commun.* **2015**, *51*, 4447–4450; c) K. Narsimhan, K. Iyoki, K. Dinh, Y. Román-Leshkov, *ACS Cent. Sci.* **2016**, *2*, 424–429; d) B. Ipek, M. J. Wulfers, H. Kim, F. Göltl, I. Hermans, J. P. Smith, K. S. Booksh, C. M. Brown, R. F. Lobo, *ACS Catal.* **2017**, *7*, 4291–4303; e) A. I. Olivos-Suarez, À. Szécsényi, E. J. M. Hensen, J. Ruiz-Martinez, E. A. Pidko, J. Gascon, *ACS Catal.* **2016**, *6*, 2965–2981; f) K. T. Dinh, M. M. Sullivan, P. Serna, R. J. Meyer, M. Dincă, Y. Román-Leshkov, *ACS Catal.* **2018**, *8*, 8306–8313.
[113] P. Tomkins, M. Ranocchiari, J. A. van Bokhoven, *Acc. Chem. Res.* **2017**, *50*, 418–425.
[114] a) C. Hammond, M. M. Forde, M. H. Ab Rahim, A. Thetford, Q. He, R. L. Jenkins, N. Dimitratos, J. A. Lopez-Sanchez, N. F. Dummer, D. M. Murphy, A. F. Carley, S. H. Taylor, D. J. Willock, E. E. Stangland, J. Kang, H. Hagen, C. J. Kiely, G. J. Hutchings, *Angew. Chem. Int. Ed.* **2012**, *51*, 5129–5133; *Angew. Chem.* **2012**, *124*, 5219–5223; b) N. V. Beznis, B. M. Weckhuysen, J. H. Bitter, *Catal. Lett.* **2010**, *136*, 52–56; c) J. J. Shan, W. X. Huang, L. Nguyen, Y. Yu, S. R. Zhang, Y. Y. Li, A. I. Frenkel, F. Tao, *Langmuir* **2014**, *30*, 8558–8569; d) J. Xu, A. Zheng, X. Wang, G. Qi, J. Su, J. Du, Z. Gan, J. Wu, W. Wang, F. Deng, *Chem. Sci.* **2012**, *3*, 2932–2940.
[115] B. E. R. Snyder, P. Vanelderen, M. L. Bols, S. D. Hallaert, L. H. Böttger, L. Ungur, K. Pierloot, R. A. Schoonheydt, B. F. Sels, E. I. Solomon, *Nature* **2016**, *536*, 317–321.
[116] a) J. S. Woertink, P. J. Smeets, M. H. Groothaert, M. A. Vance, B. F. Sels, R. A. Schoonheydt, E. I. Solomon, *Proc. Natl. Acad. Sci. U.S.A.* **2009**, *106*, 18908–18913; b) K. D. Vogiatzis, G. Li, E. J. M. Hensen, L. Gagliardi, E. A. Pidko, *J. Phys. Chem. C* **2017**, *121*, 22295–22302.
[117] M. H. Mahyuddin, T. Tanaka, Y. Shiota, A. Staykov, K. Yoshizawa, *ACS Catal.* **2018**, *8*, 1500–1509.
[118] V. L. Sushkevich, D. Palagin, M. Ranocchiari, J. A. van Bokhoven, *Science* **2017**, *356*, 523–527.
[119] Z.-J. Zhao, A. Kulkarni, L. Vilella, J. K. Nørskov, F. Studt, *ACS Catal.* **2016**, *6*, 3760–3766.
[120] R. Oord, J. E. Schmidt, B. M. Weckhuysen, *Catal. Sci. Technol.* **2018**, *8*, 1028–1038.
[121] A. R. Kulkarni, Z.-J. Zhao, S. Siahrostami, J. K. Nørskov, F. Studt, *ACS Catal.* **2016**, *6*, 6531–6536.
[122] D. K. Pappas, E. Borfecchia, M. Dyballa, I. A. Pankin, K. A. Lomachenko, A. Martini, M. Signorile, S. Teketel, B. Arstad, G. Berlier, C. Lamberti, S. Bordiga, U. Olsbye, K. P. Lillerud, S. Svelle, P. Beato, *J. Am. Chem. Soc.* **2017**, *139*, 14961–14975.
[123] S. Grundner, W. Luo, M. Sanchez-Sanchez, J. A. Lercher, *Chem. Commun.* **2016**, *52*, 2553–2556.
[124] a) S. D. Hallaert, M. L. Bols, P. Vanelderen, R. A. Schoonheydt, B. F. Sels, K. Pierloot, *Inorg. Chem.* **2017**, *56*, 10681–10690; b) B. E. R. Snyder, L. H. Böttger, M. L. Bols, J. J. Yan, H. M. Rhoda, A. B. Jacobs, M. Y. Hu, J. Zhao, E. E. Alp, B. Hedman, K. O. Hodgson, R. A. Schoonheydt, B. F. Sels, E. I. Solomon, *Proc. Natl. Acad. Sci. U.S.A.* **2018**, *115*, 4565–4570.
[125] a) M. H. Mahyuddin, Y. Shiota, A. Staykov, K. Yoshizawa, *Inorg. Chem.* **2017**, *56*, 10370–10380; b) M. H. Mahyuddin, A. Staykov, Y. Shiota, M. Miyanishi, K. Yoshizawa, *ACS Catal.* **2017**, *7*, 3741–3751.
[126] B. D. Montejo-Valencia, Y. J. Pagán-Torres, M. M. Martínez-Iñesta, M. C. Curet-Arana, *ACS Catal.* **2017**, *7*, 6719–6728.
[127] X. Solans-Monfort, M. Sodupe, J. Eckert, *J. Phys. Chem. C* **2010**, *114*, 13926–13934.
[128] A. A. Latimer, A. R. Kulkarni, H. Aljama, J. H. Montoya, J. S. Yoo, C. Tsai, F. Abild-Pedersen, F. Studt, J. K. Nørskov, *Nat. Mater.* **2016**, *16*, 225–229.
[129] A. A. Latimer, A. Kakekhani, A. R. Kulkarni, J. K. Nørskov, *ACS Catal.* **2018**, 6894–6907.
[130] T. Z. H. Gani, H. J. Kulik, *ACS Catal.* **2018**, *8*, 975–986.
[131] C. Liu, G. Li, E. A. Pidko, *Small Methods* **2018**, 1800266.
[132] K. A. Lomachenko, E. Borfecchia, C. Negri, G. Berlier, C. Lamberti, P. Beato, H. Falsig, S. Bordiga, *J. Am. Chem. Soc.* **2016**, *138*, 12025–12028.
[133] F. Gao, D. Mei, Y. Wang, J. Szanyi, C. H. F. Peden, *J. Am. Chem. Soc.* **2017**, *139*, 4935–4942.
[134] C. Paolucci, I. Khurana, A. A. Parekh, S. Li, A. J. Shih, H. Li, J. R. Di Iorio, J. D. Albarracin-Caballero, A. Yezerets, J. T. Miller, W. N. Delgass, F. H. Ribeiro, W. F. Schneider, R. Gounder, *Science* **2017**, *357*, 898–903.
[135] a) G. L. Price, V. Kanazirev, *J. Catal.* **1990**, *126*, 267–278; b) J. A. Biscardi, E. Iglesia, *Catal. Today* **1996**, *31*, 207–231; c) S. M. T. Almutairi, B. Mezari, P. C. M. M. Magusin, E. A. Pidko, E. J. M. Hensen, *ACS Catal.* **2012**, *2*, 71–83.
[136] a) J. A. Biscardi, E. Iglesia, *J. Catal.* **1999**, *182*, 117–128; b) V. B. Kazansky, I. R. Subbotina, N. Rane, R. A. van Santen, E. J. M. Hensen, *Phys. Chem. Chem. Phys.* **2005**, *7*, 3088–3092.
[137] a) J. A. Biscardi, E. Iglesia, *Phys. Chem. Chem. Phys.* **1999**, *1*, 5753–5759; b) P. L. De Cola, R. Gläser, J. Weitkamp, *Appl. Catal. A* **2006**, *306*, 85–97; c) A. A. Shubin, G. M. Zhidomirov, A. L. Yakovlev, R. A. van Santen, *J. Phys. Chem. B* **2001**, *105*, 4928–4935.
[138] E. A. Pidko, R. A. van Santen, *J. Phys. Chem. C* **2007**, *111*, 2643–2655.
[139] E. A. Pidko, R. A. van Santen, *J. Phys. Chem. C* **2009**, *113*, 4246–4249.
[140] C. Hammond, M. M. Forde, M. H. A. Rahim, A. Thelford, Q. He, R. L. Jenkins, N. Dimitratos, J. A. Lopez-Sanchez, N. F. Dummer, D. M. Murphy, A. F. Carley, S. H. Taylor, D. J. Willock, E. E. Stangland, J. Kang, H. Hagen, C. J. Kiely, G. J. Hutchings, *Angew. Chem. Int. Ed.* **2012**, *51*, 5129–5133 .
[141] Á. Szécsényi, G. Li, J. Gascon, E. A. Pidko, *ACS Catal.* **2018**, *8*, 7961–7972.
[142] Y.-P. Li, M. Head-Gordon, A. T. Bell, *ACS Catal.* **2014**, *4*, 1537–1545.
[143] a) G. Yang, E. A. Pidko, E. J. M. Hensen, *ChemSusChem* **2013**, *6*, 1688–1696; b) G. Li, E. A. Pidko, E. J. M. Hensen, *Catal. Sci. Technol.* **2014**, *4*, 2241–2250.
[144] a) M. S. Holm, S. Saravanamurugan, E. Taarning, *Science* **2010**, *328*, 602–605; b) P. Y. Dapsens, C. Mondelli, J. Perez-Ramirez, *Chem. Soc. Rev.* **2015**, *44*, 7025–7043.
[145] a) N. Rai, S. Caratzoulas, D. G. Vlachos, *ACS Catal.* **2013**, *3*, 2294–2298; b) W. R. Gunther, V. K. Michaelis, R. G. Griffin, Y. Román-Leshkov, *J. Phys. Chem. C* **2016**, *120*, 28533–28544; c) B. D. Montejo-Valencia, J. L. Salcedo-Pérez, M. C. Curet-Arana, *J. Phys. Chem. C* **2016**, *120*, 2176–2186; d) V. L. Sushkevich, I. I. Ivanova, A. V. Yakimov, *J. Phys. Chem. C* **2017**, *121*, 11437–11447.
[146] M. Moliner, Y. Román-Leshkov, M. E. Davis, *Proc. Natl. Acad. Sci. U.S.A.* **2010**, *107*, 6164–6168.
[147] a) E. Taarning, C. M. Osmundsen, X. B. Yang, B. Voss, S. I. Andersen, C. H. Christensen, *Energy Environ. Sci.* **2011**, *4*, 793–804; b) C. H. Zhou, X. Xia, C. X. Lin, D. S. Tong, J. Beltramini, *Chem. Soc. Rev.* **2011**, *40*, 5588–5617.

 © 2018 The Authors. Published by Wiley-VCH Verlag GmbH & Co. KGaA

[148] a) M. Boronat, P. Concepcion, A. Corma, M. T. Navarro, M. Renz, S. Valencia, *Phys. Chem. Chem. Phys.* **2009**, *11*, 2876–2884; b) S. K. Brand, J. A. Labinger, M. E. Davis, *ChemCatChem* **2016**, *8*, 121–124.
[149] I. K. M. Yu, D. C. W. Tsang, *Bioresour. Technol.* **2017**, *238*, 716–732.Z. Wang, J. Huang, in *Production of Biofuels and Chemicals with Bifunctional Catalysts* (Eds.: Z. Fang, R. L. Smith Jr, H. Li), Springer Singapore, **2017**, pp. 99-135.
[150] E. A. Pidko, V. Degirmenci, R. A. van Santen, E. J. M. Hensen, *Angew. Chem. Int. Ed.* **2010**, *122*, 2584–2588.
[151] A. Y. Kovalevsky, L. Hanson, S. Z. Fisher, M. Mustyakimov, S. A. Mason, V. Trevor Forsyth, M. P. Blakeley, D. A. Keen, T. Wagner, H. L. Carrell, A. K. Katz, J. P. Glusker, P. Langan, *Structure* **2010**, *18*, 688–699.
[152] a) G. Li, E. A. Pidko, E. J. M. Hensen, *ACS Catal.* **2016**, 4162–4169; b) G. Li, E. A. Pidko, E. J. M. Hensen, K. Nakajima, *ChemCatChem* **2018**, *10*, 1–7.
[153] B. K. Chethana, S. H. Mushrif, *J. Catal.* **2015**, *323*, 158–164.
[154] G. Yang, L. Zhou, *ACS Catal.* **2018**, *8*, 6691–6698.
[155] Q. Zheng, J. Xu, B. Liu, K. L. Hohn, *J. Catal.* **2018**, *360*, 221–239.
[156] Y. Chu, X. Yi, C. Li, X. Sun, A. Zheng, *Chem. Sci.* **2018**, *9*, 6470–6479.
[157] C. Paolucci, A. A. Verma, S. A. Bates, V. F. Kispersky, J. T. Miller, R. Gounder, W. N. Delgass, F. H. Ribeiro, W. F. Schneider, *Angew. Chem. Int. Ed.* **2014**, *53*, 11828–11833; *Angew. Chem.* **2014**, *126*, 12022–12027.
[158] M. W. Schreiber, C. P. Plaisance, M. Baumgärtl, K. Reuter, A. Jentys, R. Bermejo-Deval, J. A. Lercher, *J. Am. Chem. Soc.* **2018**, *140*, 4849–4859.
[159] P. Gao, Q. Wang, J. Xu, G. Qi, C. Wang, X. Zhou, X. Zhao, N. Feng, X. Liu, F. Deng, *ACS Catal.* **2018**, *8*, 69–74.
[160] A. Rimola, M. Sodupe, P. Ugliengo, *J. Am. Chem. Soc.* **2007**, *129*, 8333–8344.
[161] C. Wang, Y. Chu, J. Xu, Q. Wang, G. Qi, P. Gao, X. Zhou, F. Deng, *Angew. Chem. Int. Ed.* **2018**, *57*, 10197–10201; *Angew. Chem.* **2018**, *130*, 10354–10358.
[162] G. G. Hammes, S. J. Benkovic, S. Hammes-Schiffer, *Biochem.* **2011**, *50*, 10422–10430.
[163] a) M. D. Wodrich, X. Hu, *Nat. Rev. Chem.* **2017**, *2*, 0099; b) J. R. Khusnutdinova, D. Milstein, *Angew. Chem. Int. Ed.* **2015**, *54*, 12236–12273; *Angew. Chem.* **2015**, *127*, 12406–12445.
[164] a) A. Comas-Vives, M. Valla, C. Coperet, P. Sautet, *ACS Cent. Sci.* **2015**, *1*, 313–319; b) I. A. Popov, E. Jimenez-Izal, A. N. Alexandrova, A. I. Boldyrev, *J. Phys. Chem. C* **2018**, *122*, 11933–11937.
[165] a) W. Gao, Z. D. Hood, M. Chi, *Acc. Chem. Res.* **2017**, *50*, 787–795; b) F. R. Negreiros, G. Barcaro, L. Sementa, A. Fortunelli, *C. R. Chim.* **2014**, *17*, 625–633; c) A. Halder, L. A. Curtiss, A. Fortunelli, S. Vajda, *J. Chem. Phys.* **2018**, *148*, 110901; d) L. Liu, A. Corma, *Chem. Rev.* **2018**, *118*, 4981–5079; e) T. K. Slot, D. Eisenberg, G. Rothenberg, *ChemCatChem* **2018**, *10*, 2119–2124.
[166] a) E. A. Pidko, R. A. van Santen, *Int. J. Quantum Chem.* **2010**, *110*, 210–220; b) B. M. Szyja, D. Smykowski, J. Szczygieł, E. J. M. Hensen, E. A. Pidko, *ChemCatChem* **2016**, *8*, 2500–2507.
[167] L. Rubinovich, M. Polak, *Nano Lett.* **2013**, *13*, 2247–2251.
[168] E. A. Pidko, *ACS Catal.* **2017**, *7*, 4230–4234.
[169] a) E. Persch, O. Dumele, F. Diederich, *Angew. Chem. Int. Ed.* **2015**, *54*, 3290–3327; *Angew. Chem.* **2015**, *127*, 3341–3382; b) V. L. Schramm, *Acc. Chem. Res.* **2015**, *48*, 1032–1039.
[170] a) S. C. L. Kamerlin, P. K. Sharma, Z. T. Chu, A. Warshel, *Proc. Natl. Acad. Sci. U.S.A.* **2010**, *107*, 4075–4080; b) P. Schopf, M. J. L. Mills, A. Warshel, *Proc. Natl. Acad. Sci. U.S.A.* **2015**, *112*, 4328–4333.
[171] a) H. Hattori, *Chem. Rev.* **1995**, *95*, 537–558; b) A. L. de Lima, C. M. Ronconi, C. J. A. Mota, *Catal. Sci. Technol.* **2016**, *6*, 2877–2891.
[172] a) R. C. Deka, R. Kinkar Roy, K. Hirao, *Chem. Phys. Lett.* **2004**, *389*, 186–190; b) R. C. Deka, R. Kinkar Roy, K. Hirao, *Chem. Phys. Lett.* **2000**, *332*, 576–582; c) G. D. Pirngruber, P. Raybaud, Y. Belmabkhout, J. Čejka, A. Zukal, *Phys. Chem. Chem. Phys.* **2010**, *12*, 13534–13546.
[173] a) P. Mignon, E. A. Pidko, R. A. Van Santen, P. Geerlings, R. A. Schoonheydt, *Chem. Eur. J.* **2008**, *14*, 5168–5177; b) E. A. Pidko, P. Mignon, P. Geerlings, R. A. Schoonheydt, R. A. van Santen, *J. Phys. Chem. C* **2008**, *112*, 5510–5519.
[174] a) P. Nachtigall, M. R. Delgado, D. Nachtigallova, C. O. Arean, *Phys. Chem. Chem. Phys.* **2012**, *14*, 1552–1569; b) K. S. Walton, M. B. Abney, M. Douglas LeVan, *Microporous Mesoporous Mater.* **2006**, *91*, 78–84.
[175] a) E. Garrone, R. Bulánek, K. Frolich, C. Otero Areán, M. Rodríguez Delgado, G. T. Palomino, D. Nachtigallová, P. Nachtigall, *J. Phys. Chem. B* **2006**, *110*, 22542–22550; b) D. Nachtigallová, O. Bludský, C. Otero Areán, R. Bulánek, P. Nachtigall, *Phys. Chem. Chem. Phys.* **2006**, *8*, 4849–4852.
[176] a) M. Shamsuzzoha, Y. H. Kim, W. T. Lim, *J. Phys. Chem. C* **2011**, *115*, 17750–17760; b) R. R. Poissant, Y. Huang, R. A. Secco, *Microporous Mesoporous Mater.* **2004**, *74*, 231–238; c) J. Zhu, N. Trefiak, T. Woo, Y. Huang, *Microporous Mesoporous Mater.* **2008**, *114*, 474–484.
[177] Y. H. Yeom, A. N. Kim, Y. Kim, S. H. Song, K. Seff, *J. Phys. Chem. B* **1998**, *102*, 6071–6077.
[178] E. Kemner, I. M. d. Schepper, G. J. Kearley, *Chem. Commun.* **2001**, 2466–2467.
[179] W. N. P. van der Graaff, C. H. L. Tempelman, E. A. Pidko, E. J. M. Hensen, *Catal. Sci. Technol.* **2017**, *7*, 3151–3162.
[180] E. A. Pidko, R. A. van Santen, *J. Phys. Chem. B* **2006**, *110*, 2963–2967.
[181] a) R. Y. Rohling, I. C. Tranca, E. J. M. Hensen, E. A. Pidko, *J. Phys. Chem. C* **2018**, *122*, 14733–14743; b) R. Y. Rohling, E. J. M. Hensen, E. A. Pidko, *ChemPhysChem* **2018**, *19*, 446–458; c) R. Y. Rohling, E. Uslamin, B. Zijlstra, I. C. Tranca, I. A. W. Filot, E. J. M. Hensen, E. A. Pidko, *ACS Catal.* **2018**, *8*, 760–769.
[182] A. E. Settle, L. Berstis, N. A. Rorrer, Y. Roman-Leshkóv, G. T. Beckham, R. M. Richards, D. R. Vardon, *Green Chem.* **2017**, *19*, 3468–3492.
[183] a) M. Bergeler, G. N. Simm, J. Proppe, M. Reiher, *J. Chem. Theory Comput.* **2015**, *11*, 5712–5722; b) Z. W. Ulissi, A. J. Medford, T. Bligaard, J. K. Nørskov, *Nat. Commun.* **2017**, *8*, 14621; c) S. D. Huang, C. Shang, X. J. Zhang, Z. P. Liu, *Chem. Sci.* **2017**, *8*, 6327–6337; d) A. L. Dewyer, A. J. Argüelles, P. M. Zimmerman, *Wiley Interdiscip. Rev.: Comput. Mol. Sci.* **2018**, *8*, e1354.

Manuscript received: September 12, 2018
Revised manuscript received: November 11, 2018
Accepted manuscript online: November 12, 2018
Version of record online: ■■, ■■■

 © 2018 The Authors. Published by Wiley-VCH Verlag GmbH & Co. KGaA

REVIEWS

Caught in the midst of complexity: This Review presents an overview of recent computational studies on catalysis by cation-modified zeolites. The role of computational chemistry in addressing the structural and mechanistic complexity underlying the catalytic function of these system is discussed. The multifunctional and multisite dynamic reactive environments need to be explicitly accounted for in computational models to enable derivation of predictive structure-activity relations in zeolite catalysis.